

# TRACKING QUINTESSENCE AND COLD DARK MATTER CANDIDATES

---

**S. LOLA, C. PALLIS AND E. TZELATI**

*Department of Physics, University of Patras,  
Panepistimioupolis, GR-265 00 Patras, GREECE*

**ABSTRACT:** We study the generation of a kination-dominated phase in the context of a quintessential model with an inverse-power-law potential and a Hubble-induced mass term for the quintessence field. The presence of kination is associated with an oscillating evolution of the quintessence field and the barotropic index. We find that, in sizeable regions of the parameter space, a tracker scaling solution can be reached sufficiently early to alleviate the coincidence problem. Other observational constraints originating from nucleosynthesis, the inflationary scale, the present acceleration of the universe and the dark-energy-density parameter can be also met. The impact of this modified kination-dominated phase on the thermal abundance of cold dark matter candidates is investigated too. We find that: (i) the enhancement of the relic abundance of the WIMPs with respect to the standard paradigm, crucially depends on the hierarchy between the freeze-out temperature and the temperature at which the extrema in the evolution of the quintessence field are encountered, and (ii) the relic abundance of  $e$ -WIMPs takes its present value close to the temperature at which the earliest extremum of the evolution of the quintessence field occurs and, as a consequence, both gravitinos and axinos arise as natural cold dark matter candidates. In the case of unstable gravitinos, the gravitino constraint can be satisfied for values of the initial temperature well above those required in the standard cosmology.

**KEYWORDS:** Cosmology, Dark Matter, Dark Energy

**PACS CODES:** 98.80.Cq, 95.35.+d, 98.80.-k

**Published in *J. Cosmol. Astropart. Phys.* **11**, 017 (2009)**

---

## CONTENTS

<b>1. INTRODUCTION</b>	<b>1</b>
<b>2. TRACKING QUINTESSENCE</b>	<b>3</b>
2.1 THE QUINTESSENTIAL SET-UP . . . . .	3
2.2 IMPOSED REQUIREMENTS . . . . .	5
2.3 THE QUINTESSENTIAL DYNAMICS . . . . .	6
2.4 THE ALLOWED PARAMETER SPACE . . . . .	9
<b>3. THERMAL ABUNDANCE OF CDM CANDIDATES</b>	<b>10</b>
3.1 THE BOLTZMANN EQUATION . . . . .	11
3.2 NUMERICAL SOLUTION . . . . .	12
3.3 SEMI-ANALYTICAL APPROACH . . . . .	12
<b>4. CDM FROM THERMAL PRODUCTION OF WIMPs</b>	<b>15</b>
4.1 THE ENHANCEMENT OF $\Omega_\chi h^2$ . . . . .	15
4.2 RESTRICTIONS IN THE $m_\chi - \langle\sigma v\rangle$ PLANE . . . . .	16
<b>5. CDM FROM THERMAL PRODUCTION OF <math>e</math>-WIMPs</b>	<b>17</b>
5.1 $\Omega_\chi h^2$ AS A FUNCTION OF THE FREE PARAMETERS . . . . .	18
5.2 RESTRICTIONS IN THE $m_\chi - \log \tilde{H}_I$ PLANE . . . . .	18
<b>6. CONCLUSIONS</b>	<b>21</b>
<b>A TRACKING QUINTESSENCE AND THE <math>\tilde{G}</math> CONSTRAINT</b>	<b>22</b>

## 1. INTRODUCTION

A plethora of recent data [1, 2] indicates [3] that the two major components of the present universe are *Cold Dark Matter* (CDM) and *Dark Energy* (DE) with density parameters [1]:

$$(a) \Omega_{\text{CDM}} = 0.214 \pm 0.027 \quad \text{and} \quad (b) \Omega_{\text{DE}} = 0.742 \pm 0.03, \quad (1.1)$$

at 95% *confidence level* (c.l.). Identifying the nature of these two unknown substances is one of the major challenges in modern cosmo-particle theories.

Among the natural candidates [4] to account for CDM are [5] the *weakly interacting massive particles* (WIMPs) [6, 7], with prominent representative in supersymmetric (SUSY) theories the lightest neutralino [8] and the *extremely WIMPs* ( $e$ -WIMPs) [9] with most popular representatives, the gravitino,  $\tilde{G}$ , and the axino,  $\tilde{a}$ . Assuming  $R$ -parity conservation, the *lightest SUSY particle* (LSP) is stable and can be either a WIMP or an  $e$ -WIMP, in a sizeable region of the SUSY parameter space. The interactions of WIMPs ensure that they come to chemical equilibrium with the plasma and decouple from it at a temperature  $T_F \sim (10 - 20)$  GeV. On the other hand, the interaction of  $e$ -WIMPs are *extremely* weak since they are suppressed by the reduced Planck scale,

$m_P = M_P / \sqrt{8\pi}$  (where  $M_P = 1.22 \cdot 10^{19}$  GeV is the Planck mass) in the case of  $\tilde{G}$  and by the axion decay constant,  $f_a \sim (10^{10} - 10^{12})$  GeV (for a review, see Ref. [10]) in the case of  $\tilde{a}$ . Consequently,  $e$ -WIMPs depart from chemical equilibrium very early and their relic density (created due to this early decoupling) is diluted by primordial inflation. Subsequently,  $e$ -WIMPs can be reproduced in the thermal bath through scatterings [11, 12, 13, 14] and decays [13, 15, 16] involving superpartners. For both WIMPs and  $e$ -WIMPs (hereafter denoted collectively as  $X$ ) we may have extra non-thermal contributions to their relic density,  $\Omega_X h^2$ , [17, 18], from the out-of-equilibrium decay of the *next-to-LSP* (NLSP). However, this mechanism is highly model dependent since it is sensitive to the nature of the NLSP, its decay products and the extra restrictions which have to be imposed in order to maintain the success of the standard *Big-Bang Nucleosynthesis* (BBN). Given that it does not modify the results in any essential way, other than by moderate factors, we opt to keep the analysis as generic as possible, and therefore focus on the thermal production of CDM candidates.

A particle  $X$  consists a viable CDM candidate, provided its relic density  $\Omega_X h^2$  can be confined in the region [1]

$$(a) 0.097 \lesssim \Omega_X h^2 \lesssim 0.12 \quad \text{for} \quad (b) 10 \text{ keV} < m_X < m_{\text{NLSP}} \quad (1.2)$$

where  $m_{\text{NLSP}}$  is the NLSP mass and the lower bound on  $m_X$  comes from the fact that lower  $m_X$ 's cannot explain [19] the observed early reionization [1]. Clearly, the  $\Omega_X h^2$  calculation crucially depends on the assumption on the dominant component of the universe during the decoupling of WIMPs or the reproduction of  $e$ -WIMPs. In the *standard cosmological scenario* (SC) we assume that primordial inflation is followed by the *radiation dominated* (RD) epoch. However, our current knowledge of the history of the universe before BBN, also allows for other possibilities (see, e.g., [20, 21, 22]). Among them, an interesting alternative is provided by the presence of a *kination dominated* (KD) [23] post-inflationary era, which enhances the thermal abundance of WIMPs [20, 24, 25, 26] and significantly reduces thermal abundance of  $e$ -WIMPs [32] *with respect to* (w.r.t) their values in the SC.

The existence of a KD era is an open possibility in the framework of *quintessential scenaria* (QS). Quintessence [27] (for reviews, see Ref. [28]) is a scalar field, slowly evolving today, which can provide the required amount of the present vacuum energy and therefore explain (at least at the classical level) the other major component of the universe, the DE. Kination is also an indispensable ingredient of the quintessential inflationary scenaria [29, 30, 31]. In recent papers [26, 32] we considered the creation of a KD era in the context of the exponential quintessential model [33, 34], taking into account a number of relevant phenomenological requirements. Although this model can reproduce a viable present-day cosmology in conjunction with the domination of an early KD era, for a reasonable region of initial conditions [35], it does not possess a tracker-type solution [24, 36], where quintessence is able to reach the required value today starting from a very wide set of initial conditions in the remote past. This attractive behavior occurs in models with inverse power-law potentials, which are naturally expected in high energy particle physics models [38]. In this way the so-called ‘‘coincidence’’ or ‘‘why now’’ problem, related to the fact that the quintessential energy density is such that it is dominating the cosmic expansion right now, is addressed. However, within the minimal realizations of these models, these positive features do not coexist with the presence of an early KD era [36, 39].

In the current work, we reconsider the generation of an early KD era in the context of tracking quintessence, switching on a Hubble-induced time dependent mass term for the quintessence field, along the lines of Ref. [39] (see also Ref. [40, 41, 42]). The paper is structured as follows: In Sec. 2, we show that a KD era within this framework, is characterized by an oscillatory evolution of the quintessence field and the barotropic index. Observationally acceptable values for the latter at present times can be obtained for relatively low values of the exponent in the potential [43]. Other restrictions arising from BBN, the inflationary scale and the DE density parameter can also be met in a wide range of the parametric space, which turns out to have a band structure. In Sec. 3, we investigate the impact of this KD era on the thermal abundance of WIMPs and  $e$ -WIMPs, solving both numerically and semi-analytically the relevant Boltzmann equations. We find that, if  $X$  is a WIMP,  $\Omega_X h^2$  depends crucially on the hierarchy between the freeze-out temperature and the temperature at which the extrema in the evolution of the quintessence field are encountered. On the other hand, if  $X$  is an  $e$ -WIMP,  $\Omega_X h^2$  is determined mainly at the temperature where the first extremum (after the onset of KD era) in the evolution of the quintessence field occurs. In Sec. 4 and 5 respectively, we study the dependence of  $\Omega_X h^2$  on the free parameters of the theory, and identify the allowed parameter space for WIMPs and  $e$ -WIMPs. Our conclusions are summarized in Sec. 6. For completeness, we also discuss the cosmology of unstable  $\tilde{G}$  within our QS in Appendix A.

Throughout the text, brackets are used by applying disjunctive correspondence. Natural units are assumed for the Planck's and Boltzmann's constants and for the velocity of light ( $\hbar = c = k_B = 1$ ). The subscript or superscript "0" refers to present-day values (except in the coefficient  $\bar{V}_0$ ) and  $\log [\ln]$  stands for logarithm with basis 10 [ $e$ ]. Finally, we assume that the domain wall number [10] is equal to 1.

## 2. TRACKING QUINTESSENCE

In this section we outline the several aspects of tracking quintessence (Sec. 2.1) and the various observational restrictions that have to be imposed (Sec. 2.2). We then highlight the scalar field dynamics in Sec. 2.3 and describe the allowed parameter space of our QS in Sec. 2.4.

### 2.1 THE QUINTESSENTIAL SET-UP

We present below the equations which govern the evolution of the quintessence field (Sec. 2.1.1) and the method we use in order to solve them numerically (Sec. 2.1.2).

**2.1.1 RELEVANT EQUATIONS.** We assume the existence of a spatially homogeneous scalar field  $q$  (not to be confused with the deceleration parameter [3]) which obeys the equation:

$$\ddot{q} + 3H\dot{q} + V_{,q} = 0, \quad \text{where } V = V_a + V_b \quad \text{with } V_a = \frac{M^{4+a}}{q^a} \quad \text{and } V_b = \frac{b}{2} H^2 q^2, \quad (2.1)$$

is the adopted potential for the field  $q$  with  $M$  a mass scale and  $,q$  [dot] stands for the derivative w.r.t  $q$  [the cosmic time,  $t$ ]. The main feature of  $V_a$  is the existence of tracker solutions, which are attractors [36, 37] in field space, while  $V_b$  (with  $b$  of order unity) expresses a quite generic interaction term which arises e.g. due to non-canonical terms of the Kähler potential of  $q$  [40, 41]. Similar interactions [42] arise due to the thermal effects as well. As shown in Ref. [39] and verified

in Sec. 2.4, a mild tuning of the coefficient  $b$  enlarges the configuration space that leads to the desirable insensitivity to the initial conditions, without modifying the behavior of the field today.

The Hubble expansion parameter  $H$  in Eq. (2.1) is given by

$$H = \sqrt{\rho_q + \rho_R + \rho_M} / \sqrt{3}m_{\text{P}} \quad \text{with} \quad \rho_q = \frac{1}{2}\dot{q}^2 + V, \quad (2.2)$$

the energy density of  $q$ . The energy density of radiation,  $\rho_R$ , can be evaluated as a function of temperature,  $T$ , whilst the energy density of matter,  $\rho_M$ , with reference to its present-day value:

$$\rho_R = \frac{\pi^2}{30}g_{\rho^*} T^4 \quad \text{and} \quad \rho_M R^3 = \rho_{M0} R_0^3 \quad (2.3)$$

with  $R$  the scale factor of the universe. Assuming no entropy production due to the domination of  $q$  or another field, the entropy density,  $s$ , satisfies the equation

$$sR^3 = s_0 R_0^3 \quad \text{where} \quad s = \frac{2\pi^2}{45}g_{s^*} T^3, \quad (2.4)$$

where  $g_{\rho^*}(T)$  [ $g_{s^*}(T)$ ] is the energy [entropy] effective number of degrees of freedom at temperature  $T$ . Their precise numerical values are evaluated by using the tables included in public packages [46], assuming the particle spectrum of the Minimal SUSY Standard Model.

**2.1.2 NUMERICAL INTEGRATION.** The numerical integration of Eq. (2.1) is facilitated by converting the time derivatives to derivatives w.r.t the logarithmic time [35] which is defined as a function of the redshift  $z$ :

$$\tau = \ln(R/R_0) = -\ln(1+z). \quad (2.5)$$

Changing the differentiation and introducing the following dimensionless quantities:

$$\bar{\rho}_R = \rho_R/\rho_{c0}, \quad \bar{\rho}_M = \rho_M/\rho_{c0}, \quad \bar{V}_a = V_a/\rho_{c0}, \quad \bar{H} = H/H_0, \quad \text{and} \quad \bar{q} = q/\sqrt{3}m_{\text{P}}, \quad (2.6)$$

Eq. (2.1) turns out to be equivalent to the system of two first-order equations:

$$\bar{Q} = \bar{H}\bar{q}' \quad \text{and} \quad \bar{H}\bar{Q}' + 3\bar{H}\bar{Q} + b\bar{H}^2\bar{q} + \frac{b}{2}\bar{H}^2\bar{q}\bar{q}^2 + \bar{V}_{a,\bar{q}} = 0, \quad (2.7)$$

$$\text{where} \quad \bar{H}^2 = \frac{1}{1 - b\bar{q}^2/2} \left( \frac{1}{2}\bar{Q}^2 + \bar{\rho}_R + \bar{V}_a + \bar{\rho}_M \right). \quad (2.8)$$

Here, ‘‘prime’’ denotes derivative w.r.t.  $\tau$  and  $M$  can be expressed in terms of the dimensionless quantities as follows

$$M = \left( (\sqrt{3}m_{\text{P}})^a \bar{V}_0 \rho_{c0} \right)^{1/(4+a)} \quad \text{with} \quad \bar{V}_a = \bar{V}_0/\bar{q}^a. \quad (2.9)$$

In our numerical calculation, we use the following values:

$$\rho_{c0} \simeq 8.1 \cdot 10^{-47} h^2 \text{ GeV}^4, \quad \text{with} \quad h = 0.72, \quad \bar{\rho}_{M0} = 0.26 \quad \text{and} \quad T_0 = 2.35 \cdot 10^{-13} \text{ GeV}. \quad (2.10)$$

We have also  $H_0 = 2.13 \cdot 10^{-42} h \text{ GeV}$  and from Eq. (2.3) we get  $\bar{\rho}_{R0} = 8.04 \cdot 10^{-5}$ .

Eq. (2.8) can be solved numerically if two initial conditions are specified at an initial logarithmic time  $\tau_I$ , which corresponds to a temperature  $T_I$  defined as the maximal  $T$  after the end of primordial inflation, assuming instantaneous reheating. We take  $q(\tau_I) = 10^{-2}$  throughout our investigation, without any loss of generality (see below) and let as a free parameter  $\bar{H}_I$  (which practically

coincides with  $\bar{Q}(\tau_1)/\sqrt{2}$  since we require a complete domination of kination at early times as we describe below). To test our model against observations we extract the density parameters of the  $q$ -field, radiation and matter,

$$\Omega_i = \rho_i/(\rho_q + \rho_R + \rho_M), \quad \text{where } i = q, R \text{ and } M, \quad (2.11)$$

respectively, and the equation-of-state parameter of the  $q$ -field,  $w_q$ ,

$$w_q = \frac{P_q}{\rho_q} \quad \text{where } \bar{P}_q = \frac{1}{2}\bar{Q}^2 - \bar{V}_a - \frac{b}{2}\bar{H}^2\bar{q}^2 \quad \text{and} \quad \bar{\rho}_q = \frac{1}{2}\bar{Q}^2 + \bar{V}_a + \frac{b}{2}\bar{H}^2\bar{q}^2, \quad (2.12)$$

with  $P_q$  the pressure of  $q$  and  $\bar{P}_q = P_q/\rho_{c0}$ .

## 2.2 IMPOSED REQUIREMENTS

We impose on our quintessential model the following requirements:

**2.2.1 CONSTRAINT OF INITIAL DOMINATION OF KINATION.** As stressed in the introduction, we focus on the range of parameters that ensures the initial domination of the  $q$ -kinetic energy. This requirement can be quantified as follows:

$$\Omega_q^I = \Omega_q(T_I) = 1. \quad (2.13)$$

**2.2.2 NUCLEOSYNTHESIS CONSTRAINT.** The presence of  $\rho_q$  has to respect the successful predictions of BBN, which commences at about  $\tau_{\text{BBN}} = -22.5$  corresponding to  $T_{\text{BBN}} = 1 \text{ MeV}$  [44]. Taking into account the most up-to-date analysis of Ref. [44], we adopt a rather conservative upper bound on  $\Omega_q(\tau_{\text{BBN}})$ , less restrictive than that of Ref. [45]. Namely, we require:

$$\Omega_q^{\text{BBN}} = \Omega_q(\tau_{\text{BBN}}) \leq 0.21 \quad (95\% \text{ c.l.}) \quad (2.14)$$

where 0.21 corresponds to additional effective neutrinos species  $\delta N_\nu < 1.6$  [44]. We do not consider extra contribution in the left hand side of eq. (2.14), due to the energy density of the gravitational waves [48] generated during a possible former transition from inflation to KD epoch [29]. The reason is that inflation could be driven by another field different to  $q$  and so, any additional constraint arisen from that period would be highly model dependent. Nevertheless, inflation can provide a useful constraint for the parameters of our model as we discuss below.

**2.2.3 INFLATIONARY CONSTRAINT.** Recent data [1] strongly favors that the universe underwent an early inflationary phase. Assuming that this phase is responsible for the generation of the power spectrum of the curvature scalar  $P_s$  and tensor  $P_t$  perturbations, an upper bound on the inflationary potential  $V_I$  and consequently on  $H_I$  can be obtained [49]. More specifically, imposing the conservative restriction  $r = P_t/P_s \lesssim 1$ , and using the observational normalization of  $P_s$  [1] we get

$$H_I \lesssim \frac{\pi}{\sqrt{2}} m_{\text{P}} P_{s*}^{1/2} \Rightarrow H_I \lesssim 2.65 \cdot 10^{14} \text{ GeV} \Rightarrow \bar{H}_I \lesssim 1.72 \cdot 10^{56} \quad (2.15)$$

where \* means that  $P_{s*}$  is measured at the pivot scale  $k_* = 0.002/\text{Mpc}$ .

**2.2.4 DE-DENSITY AND COINCIDENCE CONSTRAINT.** These two requirements can be addressed if (i) the present value of  $\rho_q, \rho_{q0}$ , is compatible with the preferred range of Eq. (1.1b) and (ii)  $\rho_q$  has already reached the tracking behavior. The two conditions can be implemented [39] if

$$(a) \Omega_{q0} = \bar{\rho}_{q0} = 0.74 \text{ and } (b) d^2V(\tau = 0)/dq^2 \simeq H_0^2, \quad (2.16)$$

where we restrict ourselves to the central experimental value of  $\Omega_{q0}$ , since, this choice does not affect crucially our results on the CDM abundance.

**2.2.5 ACCELERATION CONSTRAINT.** A successful quintessential scenario has to account for the present-day acceleration of the universe, i.e. [1],

$$-1.12 \leq w_q(0) \leq -0.86 \text{ (95\% c.l.)}. \quad (2.17)$$

In our case, we end up with eternal acceleration ( $w_q < -1/3$  for  $\tau > 0$ ).

Let us finally note that the results obtained on the age of the universe  $t_0$  and the redshift of the transition from deceleration to acceleration,  $z_t$ , are marginally consistent with the experimental data, according to which  $t_0 = (13.69 \pm 0.26)$  Gyr and  $z_t = 0.46 \pm 0.26$  at 95% c.l. We do not impose the experimental data on these quantities as absolute constraints, due to the observational uncertainties in their measurement.

### 2.3 THE QUINTESSENTIAL DYNAMICS

The cosmological evolution of the various quantities involved in the model as a function of  $\tau$  is illustrated in Fig. 1 for  $\bar{q}_1 = 0.01$ ,  $a = 0.5$ ,  $b = 0.2$ ,  $T_1 = 10^9$  GeV ( $\tau_1 \simeq -51.2$ ) and  $\bar{H}_1 = 1.7 \cdot 10^{52}$  ( $\Omega_q^{\text{BBN}} = 0.01$  and  $\bar{V}_0 = 9 \cdot 10^8$  or  $M = 4.8$  eV). For comparison we also depict by dotted lines the evolution of certain quantities as a function of  $\tau$  for  $b = 0$ ,  $\bar{V}_0 = 8.8 \cdot 10^9$  (or  $M = 8$  eV) and the same residual parameters. In particular:

- In Fig. 1-(a), we present  $\log \bar{\rho}_i$  versus  $\tau$  for  $b = 0.2$  (solid lines) and  $b = 0$  (dotted lines), and for  $i = q$  (bold black lines),  $i = R + M$  (light gray lines) and  $i = A$  (thin black lines). Here,  $\bar{\rho}_q$  is computed by inserting in the last equation of Eq. (2.12) the numerical solution of Eq. (2.8). The quantity  $\bar{\rho}_{R+M} = \bar{\rho}_R + \bar{\rho}_M$  is given by Eq. (2.3), and  $\bar{\rho}_A$  is the dimensionless energy density of the attractor solution (see Sec. 2.3.3 for details).
- In Fig. 1-(b) [Fig. 1-(c)], we display  $q$  [ $q'$ ] versus  $\tau$  for  $b = 0.2$  (solid line) and  $b = 0$  (dotted line). We observe that for  $b = 0$ ,  $q$  grows to a value greater than  $m_P$  before it slows down. As a consequence,  $\bar{\rho}_q$  overshoots the tracker solution as shown in Fig. 1-(a). On the contrary, for  $b = 0.2$  this increase of  $q$  can be avoided and the tracker solution is reached before the present epoch.
- In Fig. 1-(d), we plot  $\Omega_i$  – with  $i = q$  (black line), R (light gray line) and M (gray line) – and  $w_q$  (dark gray line) versus  $\tau$ . We compute  $\Omega_i [w_q]$  applying Eq. (2.11) [Eq. (2.12)]. We observe that, in the presence of  $q$ , the universe undergoes successively a modified KD era, the RD era and then the matter-dominated era until the re-appearance of DE. During this KD,  $w_q$  takes oscillatory values between 1 and  $-1$  in sharp contrast to the case of a pure KD era where  $w_q = 1$  – see Ref. [26].

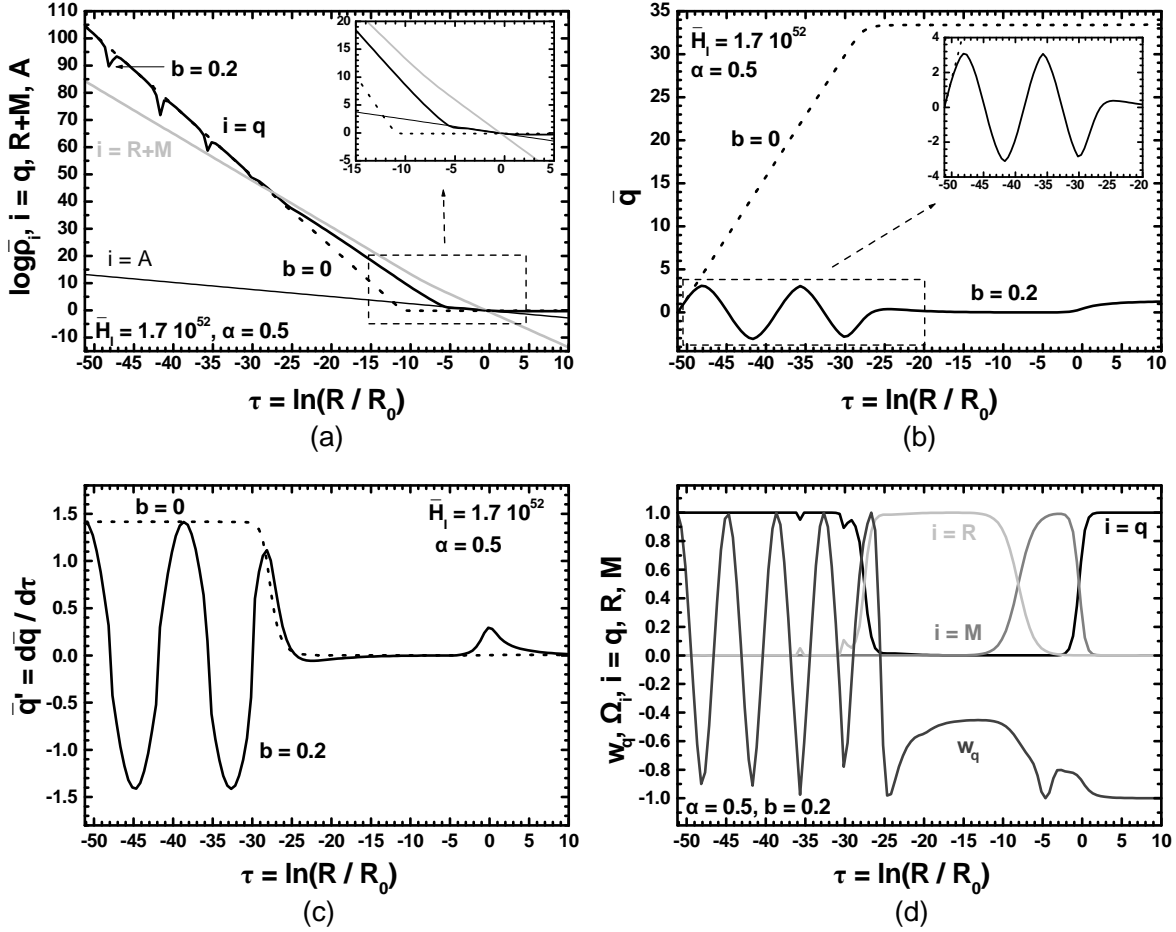


FIGURE 1: The cosmological evolution as a function of  $\tau = \ln(R/R_0)$  for  $\bar{q}_1 = 0.01$ ,  $a = 0.5$ ,  $b = 0.2$ ,  $T_1 = 10^9$  GeV ( $\tau_1 \simeq -51.2$ ) and  $\bar{H}_1 = 1.7 \cdot 10^{52}$  ( $\Omega_q^{\text{BBN}} = 0.01$  and  $\bar{V}_0 = 9 \cdot 10^8$ ) of the quantities (a)  $\log \bar{\rho}_i$  with  $i = q$  (solid black line),  $R+M$  (light gray line) and  $A$  (thin line) (b)  $\bar{q}$  (c)  $\bar{q}' (= d\bar{q}/d\tau)$  and (d)  $w_q$  (dark gray line) and  $\Omega_i$  with  $i = q$  (black line),  $R$  (light gray line) and  $M$  (gray line). For comparison we also depict by dotted lines the evolution as a function of  $\tau$  of the quantities (a)  $\log \bar{\rho}_q$  (b)  $\bar{q}$  and (c)  $\bar{q}'$  for  $a = 0.5$ ,  $b = 0$ ,  $T_1 = 10^9$  GeV ( $\tau_1 \simeq -51.2$ ),  $\bar{H}_1 = 1.7 \cdot 10^{52}$  and  $\bar{V}_0 = 8.8 \cdot 10^9$ .

To further facilitate the understanding of the quintessential dynamics we present below a qualitative approach applying the arguments of Ref. [30, 38]. In particular,  $q$  undergoes the following four phases during its evolution:

**2.3.1 KINATION DOMINATED PHASE.** During this phase, the evolution of both the universe and  $q$  is dominated by the kinetic-energy density of  $q$ . Consequently, Eq. (2.7) reads:

$$\bar{Q}' + 3\bar{Q} + b\bar{H}\bar{q} \simeq 0 \quad \text{and} \quad \bar{Q} = \bar{H}\bar{q}' \quad \text{with} \quad \bar{H} = \sqrt{\bar{\rho}_q} \simeq \bar{Q}/\sqrt{2 - b\bar{q}^2}. \quad (2.18)$$

The former equations can be integrated trivially to give:

$$\bar{q} \simeq \sqrt{\frac{2}{b}} \sin \left( \sqrt{b}(\tau - \tau_1) + \arcsin \sqrt{\frac{b}{2}} \bar{q}_1 \right) \quad \text{and} \quad \bar{Q} \simeq \bar{Q}_1 \cos \sqrt{b}(\tau - \tau_1) e^{-3(\tau - \tau_1)}. \quad (2.19)$$

Obviously, for  $b > 0$ ,  $q$  and  $Q$  are set in harmonic oscillations during the KD era. Note that for  $b \rightarrow 0$ , we recover the well-known results of a pure KD phase [26] – depicted by dotted lines in



Fig. 1-(c) and (d). In other words [39],  $V$  with  $b > 0$  acquires a (time-dependent) minimum and  $q$  is prevented from increasing sharply as in the case with  $b = 0$ . In particular,  $\bar{q}$  develops extrema at

$$\tau_{\text{ext}} \simeq \sqrt{\frac{1}{b}} \left( (2k+1) \frac{\pi}{2} - \arcsin \sqrt{\frac{b}{2} \bar{q}_I} \right) + \tau_I \quad \text{with } k = 0, 1, 2, \dots \quad (2.20)$$

On the other hand,  $\bar{q}'$  and  $\bar{Q}$  almost vanish for  $\tau = \tau_{\text{ext}}$  (given that  $\bar{q}_I \sim 0$ ). Therefore, at  $\tau \simeq \tau_{\text{ext}}$  our approximation in Eq. (2.18) fails instantaneously and  $\bar{\rho}_R$  dominates over  $\bar{Q}^2/2$ . As a consequence the  $\bar{q}$  and  $\bar{Q}$  oscillations become anharmonic and the results of Eq. (2.19) deviate from their numerical values. These deviations are enhanced as  $|\tau - \tau_I|$  increases and/or  $\bar{H}_I$  decreases. The oscillatory behavior of  $\bar{q}$  is the origin of the peaks shown on the curve of  $\bar{\rho}_q$  in Fig. 1-(a) and the oscillatory form of  $w_q$  in Fig. 1-(b). Nevertheless, the simple formula – see Ref. [26] – which estimates the point  $\tau_{\text{KR}}$  where the totally KD phase is terminated, is still valid with rather good accuracy, i.e.,

$$\tau_{\text{KR}} \simeq \tau_I + \ln \sqrt{\rho_{qI}/\rho_{RI}}. \quad (2.21)$$

For  $b = 0.2$  – and the inputs of Fig. 1 – we get numerically [analytically]  $\tau_{\text{KR}} = -27.5$  [ $\tau_{\text{KR}} = -28$ ] which corresponds to  $T_{\text{KR}} = 0.13$  GeV [ $T_{\text{KR}} = 0.2$  GeV], whereas for  $b = 0$  the numerical findings coincide with the analytic ones ( $\tau_{\text{KR}} = -28$ ).

**2.3.2 FROZEN-FIELD DOMINATED PHASE.** For  $\tau > \tau_{\text{KR}}$ , the universe becomes RD – and so  $\bar{H}^2 = \bar{\rho}_R/(1 - b\bar{q}^2/2)$  – while the evolution of  $q$  continues to be dominated by its kinetic energy density. As a consequence, Eq. (2.1) is simplified as follows:

$$\bar{q}'' + \bar{q}' + b\bar{q} + \frac{b}{2}\bar{q}\bar{q}' \simeq 0. \quad (2.22)$$

Due to the complexity of this equation, it is hard to obtain a reliable approximate solution. What we can say, however, is that, during this period, both  $q$  and  $Q$  cease to oscillate and freeze at an almost constant value. For  $b = 0.2$ ,  $\log \bar{\rho}_q$  decreases less steeply than for  $b = 0$  and thus,  $\log \bar{\rho}_q$  may join the tracker solution in time – see Fig. 1-(a).

**2.3.3 ATTRACTOR DOMINATED PHASE.** In this regime, omitting  $\ddot{q}$  and corrections of order  $b^2$ , Eq. (2.1) can be simplified as follows:

$$\bar{q}' + \frac{b}{3}\bar{q} - \frac{a\bar{V}_0}{3\bar{q}^{(a+1)}\bar{\rho}_{B0}} e^{3(1+w_B)\tau} \simeq 0 \quad \text{where } \bar{\rho}_B = \bar{\rho}_{B0} e^{-3(1+w_B)\tau} \quad (2.23)$$

is the dominant background energy density of the universe with  $w_B = 1/3$  [0] for the RD [matter-dominated] era. The solution of (2.23) can be written as

$$\bar{q}_A \simeq \left( \frac{a(a+2)\bar{V}_0}{(9+(2+b)a)\bar{\rho}_{M0}} \right)^{1/(2+a)} e^{3(1+w_B)\tau/(a+2)} \quad (2.24)$$

As a consequence [38], the system in Eq. (2.1) admits a tracking solution since the energy density of the attractor

$$\bar{\rho}_A \simeq \bar{\rho}_{Af} e^{-3(1+w_q^{\text{fp}})(\tau-\tau_{Af})} \quad \text{with } w_q^{\text{fp}} = \frac{aw_B - 2}{a+2} \quad (2.25)$$

tracks the dominant  $\bar{\rho}_B$  until  $\tau = \tau_{Af}$  where the tracking regime finishes and  $\bar{\rho}_B \simeq \bar{\rho}_A$ . Indeed,  $\bar{\rho}_A$  decreases less rapidly w.r.t  $\bar{\rho}_B$  for  $a > 0$ , since

$$\bar{\rho}_A/\bar{\rho}_B \propto e^{6(1+w_B)\tau/(a+2)} \quad (2.26)$$

As a result,  $\bar{\rho}_q$  eventually dominates and the expressions leading to the scaling solution of Eq. (2.25) can be neglected. Solving  $\bar{\rho}_M = \bar{\rho}_A$  w.r.t.  $\tau$  (since in our cases  $\bar{\rho}_B = \bar{\rho}_M$ ) we obtain the following expression for  $\tau_{Af}$ :

$$\tau_{Af} \simeq \frac{1}{6}a \ln \frac{a(2+a)}{(9+b(2+a))} + \frac{1}{3} \ln \frac{\bar{\rho}_{M0}}{\bar{V}_0}. \quad (2.27)$$

In Fig. 1-(a) we depict with a thin solid line the evolution of  $\bar{\rho}_A$  given by Eq. (2.25). For the input parameters of Fig. 1 we find that the onset of this phase takes place at  $\tau_{Ai} \simeq -3.62$  and terminates at  $\tau_{Af} = -0.4$  with  $\bar{\rho}_{Af} = 0.88$  and  $w_q^{\text{fp}} \simeq -0.81$ . We check that for  $\tau_{Ai} \leq \tau \leq \tau_{Af}$ ,  $\bar{\rho}_A/\bar{\rho}_q \simeq 0.96$ . This fact – in conjunction with the fulfillment of Eq. (2.16b) – ensures a pure domination of the attractor solution for a well-defined period, shown in more detail in the subfigure of Fig. 1-(a).

**2.3.4 VACUUM DOMINATED PHASE.** For  $\tau > \tau_{Af}$ , the universe is dominated by  $V$  and so, Eq. (2.1) can be written as

$$\bar{q}' + \frac{b}{3} \bar{q} - \frac{a}{3\bar{q}} \simeq 0 \Rightarrow \bar{q} \simeq \sqrt{\frac{a}{b}} \left( 1 - 9e^{-2b\tau/3} \frac{(a(2+a))^{ab/9}}{(9+b(2+a))^{(1+ab/9)}} \left( \frac{\bar{\rho}_{M0}}{\bar{V}_0} \right)^{2b/9} \right)^{1/2}. \quad (2.28)$$

Using the expression above for  $\bar{q}$  we can estimate  $w_q(0)$  at present through the formula

$$w_q(0) \simeq 1 - \frac{2}{1 + \bar{q}'(0)^2/2 + b\bar{q}(0)^2/2} \quad (2.29)$$

with results  $\bar{q}(0) = 0.42$  and  $w_q(0) \simeq -0.88$  for the parameters used in Fig. 1. We also obtain  $z_t = 0.76$  and  $t_0 = 13.2$  Gyr which are more or less within the experimental limits.

## 2.4 THE ALLOWED PARAMETER SPACE

The free parameters of our quintessential model are:

$$a, b, M, \tau_I \text{ (or } T_I), \bar{q}_I \text{ and } \bar{H}_I.$$

Agreement with Eq. (2.17) implies  $0 < a \leq 0.6$  (compare also with Ref. [43], where a less restrictive upper bound on  $w_q(0)$  has been imposed). The parameter  $M$  can be determined for every  $a$  through Eq. (2.9), so that Eq. (2.16a) is satisfied. The determination of  $a$  and  $M$  is independent of  $\tau_I$ ,  $\bar{q}_I$  and  $\bar{H}_I$ , provided that the tracking solution is reached in time. This property gives an idea of the stability of the tracking solutions. Note that in the case of the exponential potential, studied in Ref. [26, 32], any variation on  $\bar{q}_I$  and  $\bar{H}_I$  requires a re-adjustment of  $\bar{V}_0$  so that Eq. (2.16a) is met. On the other hand,  $\Omega_q^{\text{BBN}}$  (which influences the calculation of  $\Omega_\chi h^2$ ) does depend crucially on  $\bar{H}_I$  and  $\tau_I$  (and very weakly on  $\bar{q}_I$ ).

In Fig. 2-(a) we illustrate the allowed parameter space of our model in the  $b - \log \bar{H}_I$  plane for  $T_I = 10^9$  GeV,  $a = 0.5$  and  $\bar{q}_I = 0.01$ . In the gray shaded areas, Eqs. (2.13) - (2.17) are fulfilled. The upper boundary curves of the allowed bands come from Eq. (2.14). In the overall

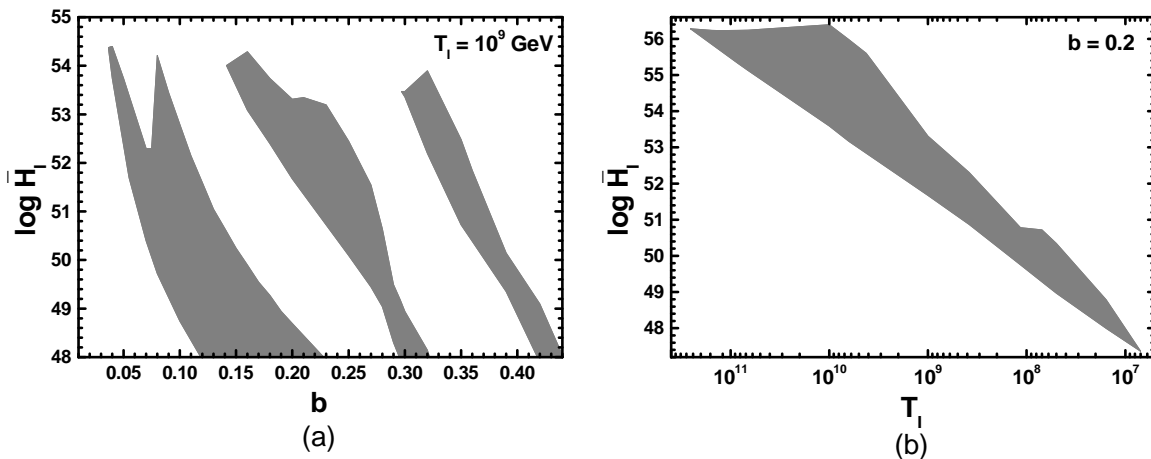


FIGURE 2: Allowed (gray shaded) region by Eqs. (2.13)-(2.17) in the (a)  $b - \log \bar{H}_I$  plane for  $T_I = 10^9$  GeV and (b)  $T_I - \log \bar{H}_I$  plane for  $b = 0.2$ . In both cases we take  $a = 0.5$  and  $\bar{q}_I = 0.01$ .

allowed region, we obtain  $10^{-6} \lesssim \Omega_q^{\text{BBN}} \lesssim 0.21$ . Note, however, that saturation of Eq. (2.14) is not possible for  $0.08 < b < 0.16$ . Clearly, the model possesses an allowed parameter space with a band structure. If  $(b, \log \bar{H}_I)$  belongs in a white [gray] band the resulting  $\bar{q}$  after the oscillatory phase turns out to be negative [positive] and thus, it cannot [can] serve as quintessence. Let us once more fix  $b = 0.2$ . For  $51.7 \lesssim \log \bar{H}_I \lesssim 53.3$ ,  $\bar{q}$  develops five extrema during its evolution – which is of the type shown in the subfigure of Fig. 1-(b) – resulting to  $\bar{q}_0 > 0$ . As  $\log \bar{H}_I$  decreases below 53.3 (where the bound of Eq. (2.14) is saturated), the amplitude of the fifth peak, which appears in the  $\bar{q}$ -evolution (at about  $\tau \simeq -24.5$ ) eventually decreases and finally this peak disappears at  $\log \bar{H}_I \simeq 51.7$  where the first allowed band terminates. For  $48.7 \lesssim \log \bar{H}_I \lesssim 51.7$ ,  $\bar{q}$  develops four extrema during its evolution, resulting to  $\bar{q}_0 < 0$ . As  $\log \bar{H}_I$  decreases below 51.7 the amplitude of the fourth peak which appears in the  $\bar{q}$ -evolution (at about  $\tau \simeq -30$ ) decreases and finally this peak disappears at  $\log \bar{H}_I \simeq 48.7$  where the second allowed band commences. Note that in the first allowed band  $\Omega_q^{\text{BBN}}$  increases with  $\bar{H}_I$  but this is not a generic rule (as in the case of a pure KD era).

Fixing  $b = 0.2$  and letting  $T_I$  vary in a range of relatively high values (motivated by the models of SUSY hybrid inflation [50]), we depict in Fig. 2-(b) the region allowed by Eqs. (2.13) - (2.17) in the  $T_I - \log \bar{H}_I$  plane for  $a = 0.5$  and  $\bar{q}_I = 0.01$ . The upper boundary of the allowed region comes from Eq. (2.15) for  $6.7 \lesssim T_I/10^{10}$  GeV  $\lesssim 25.4$  whereas for  $3.8 \lesssim T_I/10^9$  GeV  $\lesssim 67$  it arises from the condition  $\bar{q}(0) > 0$ . The same applies for the left boundary of the allowed region and several parts of its right boundary. On some parts of the latter boundary, Eq. (2.14) is also saturated. In the overall allowed region we obtain  $10^{-9} \lesssim \Omega_q^{\text{BBN}} \lesssim 0.21$ .

### 3. THERMAL ABUNDANCE OF CDM CANDIDATES

We turn now to the calculation of the thermal abundance,  $\Omega_X h^2$  of a CDM candidate,  $X$ , which can be a WIMP or an  $e$ -WIMP. If  $X$  is a WIMP we assume that it maintains kinetic and chemical equilibrium with plasma, is produced through thermal scatterings and decouples (being non-relativistic) during the KD epoch. If  $X$  is an  $e$ -WIMP, we expect that its relic abundance, due to its early decoupling from the thermal bath, is diluted after inflation at a relatively high energy scale and we compute its abundance produced through thermal scatterings and decays during the KD era. In

Sec. 3.1 we present the Boltzmann equation that governs the evolution of the  $X$  number density and then describe the procedure we employ to solve this equation numerically (Sec. 3.2) and semi-analytically (Sec. 3.3).

### 3.1 THE BOLTZMANN EQUATION

Since  $X$ 's are in kinetic equilibrium with the cosmic fluid, their number density,  $n_X$ , evolves according to the Boltzmann equation:

$$\dot{n}_X + 3Hn_X = \begin{cases} -\langle\sigma v\rangle(n_X^2 - n_X^{\text{eq}2}) & \text{if } X \text{ is WIMP,} \\ C_X n^{\text{eq}2} + \sum_i \frac{g_i}{2\pi^2} m_i^2 T K_1(m_i/T) \Gamma_i & \text{if } X \text{ is } e\text{-WIMP,} \end{cases} \quad (3.1)$$

where  $H$  is given by Eq. (2.2). Let us define the residual symbols of Eq. (3.1) separately:

**3.1.1 THE CASE OF WIMPs.** In this case,  $\langle\sigma v\rangle$  is the thermal-averaged cross section of WIMPs (hereafter denoted as  $\chi$ 's) times the velocity and  $n_\chi^{\text{eq}}$  is the equilibrium number density of  $\chi$ , which obeys the Maxwell-Boltzmann statistics:

$$n_\chi^{\text{eq}}(x) = \frac{g}{(2\pi)^{3/2}} m_\chi^3 x^{3/2} e^{-1/x} P_2\left(\frac{1}{x}\right), \quad \text{where } x = \frac{T}{m_\chi} \quad \text{and } P_n(z) = 1 + \frac{(4n^2 - 1)}{8z} \quad (3.2)$$

is a function obtained by expanding the modified Bessel function of the second kind of order  $n$  for  $x \ll 1$  ( $m_\chi$  is the mass of  $\chi$ ). Assuming that  $\chi$ 's are Majorana fermions, we set  $g = 2$  for their number of degrees of freedom. Let us clarify that  $\langle\sigma v\rangle$  can be derived from  $m_\chi$  and the residual (s)-particle spectrum, once a specific theory has been adopted. Following our strategy in Ref. [26], we treat  $m_\chi$  and  $\langle\sigma v\rangle$  as unrelated input parameters in order to keep our presentation as general as possible. Note, also that far enough from  $s$ -poles and thresholds  $\langle\sigma v\rangle$  can be expanded [5] non-relativistically as  $\langle\sigma v\rangle = a + bx$ , where  $a$  and  $b$  are constants.

**3.1.2 THE CASE OF  $e$ -WIMPs.** In this case,  $n^{\text{eq}} = \zeta(3)T^3/\pi^2$  is the equilibrium number density of the bosonic relativistic species,  $m_i$  [ $g_i$ ] is the mass [number of degrees of freedom] of the particle  $i$  and  $K_n$  is the modified Bessel function of the 2nd kind of order  $n$ . In the relativistic regime ( $T \gg m_i$ )  $C_X$  has been calculated using the *Hard Thermal Loop Approximation* [12, 14], resulting to  $C_X = C_X^{\text{HT}}$ , where

$$C_X^{\text{HT}} = \begin{cases} \frac{3\pi}{16\zeta(3)m_{\text{P}}^2} \sum_{\alpha=1}^3 \left(1 + \frac{M_\alpha^2}{3m_X^2}\right) c_\alpha g_\alpha^2 \ln\left(\frac{k_\alpha}{g_\alpha}\right) & \text{for } X = \tilde{G}, \\ \frac{108\pi g_a^2 g_3^2}{\zeta(3)} \ln\left(\frac{1.211}{g_3}\right) \quad \text{with } g_a = \frac{g^2}{32\pi^2 f_a} & \text{for } X = \tilde{a}. \end{cases} \quad (3.3)$$

Here,  $g_\alpha$  and  $M_\alpha$  (with  $\alpha = 1, 2, 3$ ) are the gauge coupling constants and gaugino masses respectively, associated with the gauge groups  $U(1)_Y$ ,  $SU(2)_L$  and  $SU(3)_C$ ,  $(k_\alpha) = (1.634, 1.312, 1.271)$  and  $(c_\alpha) = (33/5, 27, 72)$ . Note that we include the recently corrected [14] nominator (1.211) in the logarithm of  $C_{\tilde{a}}^{\text{HT}}$ . Throughout our analysis we impose universal initial conditions for the gaugino masses,  $M_\alpha(M_{\text{GUT}}) = M_{1/2}$  and gauge coupling constant unification, i.e.,  $g_\alpha(M_{\text{GUT}}) = g_{\text{GUT}}$  with  $M_{\text{GUT}} \simeq 2 \cdot 10^{16}$  GeV. Eq. (3.3) can be applied self-consistently only for  $g_\alpha(T) < 1$  or equivalently  $T > T_C = 10^4$  GeV. Towards lower  $T$ 's, non-relativistic ( $T \ll m_i$ ) contributions and  $X$  production from decays start playing an important role. These contributions have been incorporated in our

computation for the case of  $\tilde{a}$ , following the formalism of Ref. [32]. In particular, for  $T \ll m_i$ ,  $C_{\tilde{a}} = C_{\tilde{a}}^{\text{LT}}$  has been calculated numerically and  $\Gamma_i$ 's with  $i = \tilde{g}, \tilde{q}$  and  $\tilde{B}$  are taken into account [13, 15, 32] using the following benchmark values of  $m_i$ 's:

$$(m_{\tilde{g}}, m_{\tilde{q}}, m_{\tilde{B}}) = (1, 1.5, 0.3) \text{ TeV.} \quad (3.4)$$

On the other hand, in the case of  $\tilde{G}$ , we restrict ourselves to the high temperature regime (no formalism for the  $\tilde{G}$  production at low  $T$  is available to date). We do not include  $\tilde{G}$  production from sparticle decays in the plasma [16] which can change [9]  $\Omega_{\tilde{G}} h^2$  by a factor of about two but does not alter our conclusions in any essential way.

### 3.2 NUMERICAL SOLUTION

In order to find a precise numerical solution to our problem, we have to solve Eq. (3.1) together with Eq. (2.1). To this end we follow the strategy of Sec. 2.1, introducing the dimensionless quantities:

$$\bar{n}_X = n_X/\rho_{c0}^{3/4}, \quad \bar{n}_X^{\text{eq}} = n_X^{\text{eq}}/\rho_{c0}^{3/4}, \quad \bar{n}^{\text{eq}} = n^{\text{eq}}/\rho_{c0}^{3/4}, \quad \langle \overline{\sigma v} \rangle = \sqrt{3} m_{\text{P}} \rho_{c0}^{1/4} \langle \sigma v \rangle, \quad (3.5)$$

$$\bar{C}_X = \sqrt{3} m_{\text{P}} \rho_{c0}^{1/4} C_X, \quad \bar{m}_i = m_i/\rho_{c0}^{1/4}, \quad \bar{T} = T/\rho_{c0}^{1/4} \quad \text{and} \quad \bar{\Gamma}_i = \Gamma_i/H_0. \quad (3.6)$$

In terms of these quantities, Eq. (3.1) takes the following master form for numerical manipulations:

$$\bar{H} \bar{n}'_X + 3\bar{H} \bar{n}_X = \begin{cases} -\langle \overline{\sigma v} \rangle (\bar{n}_X^2 - \bar{n}_X^{\text{eq}2}) & \text{if } X \text{ is WIMP,} \\ \bar{C}_X \bar{n}^{\text{eq}2} + \sum_i \frac{g_i}{2\pi^2} \bar{\Gamma}_i \bar{m}_i^2 \bar{T} K_1(m_i/T) & \text{if } X \text{ is } e\text{-WIMP,} \end{cases} \quad (3.7)$$

where  $\bar{H}$  is given by Eq. (2.8). The integration of Eq. (3.7) is done until  $\tau_{\text{BBN}} \simeq -22.5$  (an integration until 0 gives the same result). In the case of WIMPs, we impose the initial condition  $\bar{n}_X(\tau_X) = \bar{n}_X^{\text{eq}}(\tau_X)$ , where  $\tau_X$  corresponds to the beginning ( $x = 1$ ) of the Boltzmann suppression of  $\bar{n}_X^{\text{eq}}$ . In the case of  $e$ -WIMPs, we set the initial condition  $\bar{n}_X(\tau_1) \simeq 0$ . We use  $C_X = C_X^{\text{HT}}$  if  $T_1 \gg T_C$  and  $T_{\text{KR}} \gg T_C$ . On the other hand, if  $T_1 \gg T_C$  and  $T_{\text{KR}} \ll T_C$  we integrate successively Eq. (3.7) from  $\tau_1$  to  $\tau_{\text{SUSY}} \simeq -37$  – which corresponds to  $T_{\text{SUSY}} = 1 \text{ TeV}$  – with  $C_{\tilde{a}} = C_{\tilde{a}}^{\text{HT}}$  and then from  $\tau_{\text{SUSY}}$  to  $\tau_{\text{BBN}}$  with  $C_{\tilde{a}} = C_{\tilde{a}}^{\text{LT}}$ . Finally,  $\Omega_X h^2$  is evaluated from the well-known formula:

$$\Omega_X = \rho_{X0}/\rho_{c0} = m_X s_0 Y_{X0}/\rho_{c0} \Rightarrow \Omega_X h^2 = 2.748 \cdot 10^8 Y_{X0} m_X/\text{GeV}. \quad (3.8)$$

where  $\rho_X = m_X n_X$ ,  $Y_X = n_X/s$  is the  $X$  yield and  $s_0 h^2/\rho_{c0} = 2.748 \cdot 10^8/\text{GeV}$ .

### 3.3 SEMI-ANALYTICAL APPROACH

To facilitate the understanding of our results we adapt the approach carried out in Ref. [26, 32] to our set-up. In particular, re-expressing Eq. (3.1) in terms of the variables  $Y_X$ ,  $Y_X^{\text{eq}} = n_X^{\text{eq}}/s$  and  $Y^{\text{eq}} = n^{\text{eq}}/s$  (in order to absorb the dilution term) and converting the derivatives w.r.t  $t$  to derivatives w.r.t  $\tau$ , we obtain:

$$Y'_X = y \sqrt{\frac{g_b}{g_q}} \begin{cases} (-\langle \overline{\sigma v} \rangle) (Y_X^2 - Y_X^{\text{eq}2}) & \text{if } X \text{ is WIMP,} \\ \bar{C}_X Y^{\text{eq}2} & \text{if } X \text{ is } e\text{-WIMP,} \end{cases} \quad \text{where} \quad (3.9)$$

$$y(\tau) = \frac{\bar{s}}{\sqrt{\bar{\rho}_R}} \quad \text{with} \quad \bar{s} = \frac{s}{\rho_{c0}^{3/4}}, \quad g_b = 1 - \frac{b}{2} \bar{q}^2 \quad \text{and} \quad g_q \simeq \begin{cases} 1 + \bar{Q}^2/2\bar{\rho}_R & \text{for } \tau \ll \tau_{\text{KR}}, \\ 1 & \text{for } \tau \gg \tau_{\text{KR}}. \end{cases}$$

In extracting Eq. (3.9) we keep only the first two terms in the parenthesis of Eq. (2.8) and the first term of the left hand side of Eq. (3.1) for  $e$ -WIMPs (see below). For  $g_b = 1$  (or  $b = 0$ ) [ $g_b = g_q = 1$ ], we reproduce the well-known results of the pure KD phase [of the SC]. Let us discuss how we can solve Eq. (3.9) in the two cases separately:

**3.3.1 THE CASE OF WIMPs.** An accurate approximate solution to Eq. (3.9) can be achieved, introducing the notion of freeze-out temperature,  $T_F = T(\tau_F) = x_F m_\chi$  (see, e.g., Ref. [26] and references therein), which allows us to study Eq. (3.9) in the two extreme regimes:

- For  $\tau \ll \tau_F$ ,  $Y_\chi \simeq Y_\chi^{\text{eq}}$ . In this case, it is more convenient to rewrite eq. (3.9) in terms of the variable  $\Delta(\tau) = Y_\chi(\tau) - Y_\chi^{\text{eq}}(\tau)$  as follows:

$$\Delta' = -Y_\chi^{\text{eq}'} - y \overline{\langle \sigma v \rangle} \Delta (\Delta + 2Y_\chi^{\text{eq}}) \sqrt{g_b/g_q}. \quad (3.10)$$

The freeze-out logarithmic time  $\tau_F$  can be defined by

$$\Delta(\tau_F) = \delta_F Y_\chi^{\text{eq}}(\tau_F) \Rightarrow \Delta(\tau_F) (\Delta(\tau_F) + 2Y_\chi^{\text{eq}}(\tau_F)) = \delta_F (\delta_F + 2) Y_\chi^{\text{eq}2}(\tau_F), \quad (3.11)$$

where  $\delta_F$  is a constant of order one, determined by comparing the exact numerical solution of Eq. (3.9) with the approximate one under consideration. Inserting Eq. (3.11) into Eq. (3.10), we obtain the following equation, which can be solved w.r.t  $\tau_F$  iteratively:

$$\left( \ln Y_\chi^{\text{eq}} \right)'(\tau_F) = -y_F \overline{\langle \sigma v \rangle} \delta_F (\delta_F + 2) Y_\chi^{\text{eq}}(\tau_F) \sqrt{g_b/g_q} / \sqrt{g_q} (\delta_F + 1) \quad \text{with} \quad (3.12)$$

$$y_F = y(\tau_F) \quad \text{and} \quad \left( \ln Y_\chi^{\text{eq}} \right)'(\tau) = x' \left( \frac{1}{x^2} - \frac{3}{2x} - \frac{g'_{s*}}{g_{s*}} + \frac{15}{8P_2(1/x)} \right), \quad (3.13)$$

where the  $x - \tau$  dependence can be derived from Eq. (2.4).

- For  $\tau \gg \tau_F$ ,  $Y_\chi \gg Y_\chi^{\text{eq}}$  and therefore,  $Y_\chi^2 - Y_\chi^{\text{eq}2} \simeq Y_\chi^2$ . Inserting this into Eq. (3.9) and integrating the resulting equation from  $\tau_F$  down to 0, we arrive at:

$$Y_{\chi 0} = \left( Y_{\chi F}^{-1} + J_F \right)^{-1}, \quad \text{where} \quad J_F = \int_{\tau_F}^0 d\tau \sqrt{\frac{g_b}{g_q}} y \overline{\langle \sigma v \rangle} \quad \text{and} \quad Y_{\chi F} = (\delta_F + 1) Y_\chi^{\text{eq}}(\tau_F). \quad (3.14)$$

Although not crucial, a choice  $\delta_F = 1.2 \mp 0.2$  assists us to better approach the precise numerical solution of Eq. (3.9).

Inserting Eq. (3.14) into Eq. (3.8) we can obtain  $\Omega_\chi h^2$  semianalytically. We verify that this result matches well the one found through the purely numerical integration of Eq. (3.7).

**3.3.2 THE CASE OF e-WIMPs.** In this case, we focus on the most intriguing possibility, in which  $T_I \gg T_{\text{SUSY}}$  but  $T_{\text{KR}} \ll T_{\text{SUSY}}$ . Under this assumption,  $T_I$  takes sufficient high values, as suggested by the majority of the inflationary modes (see, e.g., Ref. [50]) and  $\Omega_q^{\text{BBN}}$  naturally takes values close to its upper bound in Eq. (2.14).  $Y_{X0}$  can be derived by numerically integrating Eq. (3.9) from  $\tau = \tau_I$  until  $\tau_{\text{BBN}}$  with  $C_X = C_X^{\text{HT}}$ . This is, because  $Y_X$  is stabilized to its final value,  $Y_{X0}$ , not at the onset of the RD era – as in the case of a pure KD era [32] – but at a high temperature corresponding to  $\tau_{\text{ext}}$  for  $k = 0$  in Eq. (2.20). There, the first peak (for  $\tau > \tau_I$ ) of the  $q$  evolution takes place and therefore,  $\bar{\rho}_R$  dominates over  $\bar{\rho}_q$  instantaneously as explained in Sec. 2.3.1. Consequently,  $Y_{X0}$  decreases in our QS w.r.t its value in the SC but increases w.r.t its value in the case of a pure KD phase. To illustrate this key point we display in Fig. 3-(a) [Fig. 3-(b)] the evolution of  $\log Y_X$  for  $X = \tilde{G}$  [ $X = \tilde{a}$ ] as a function of  $\tau$  for  $T_I = 10^{10}$  GeV [ $T_I = 5 \cdot 10^7$  GeV],  $\tilde{H}_I = 10^{55}$  [ $\tilde{H}_I = 9.4 \cdot 10^{48}$ ],  $M_{1/2} = 1$  TeV [ $f_a = 10^{11}$  GeV] and  $b = 0$  (dashed line) or  $b = 0.2$  (solid line). For  $b = 0.2$  and  $m_{\tilde{G}} = 0.44$  GeV [ $m_{\tilde{a}} = 9.5$  MeV] we get  $\Omega_X h^2 = 0.11$  (with  $X = \tilde{G}$  [ $X = \tilde{a}$ ]).

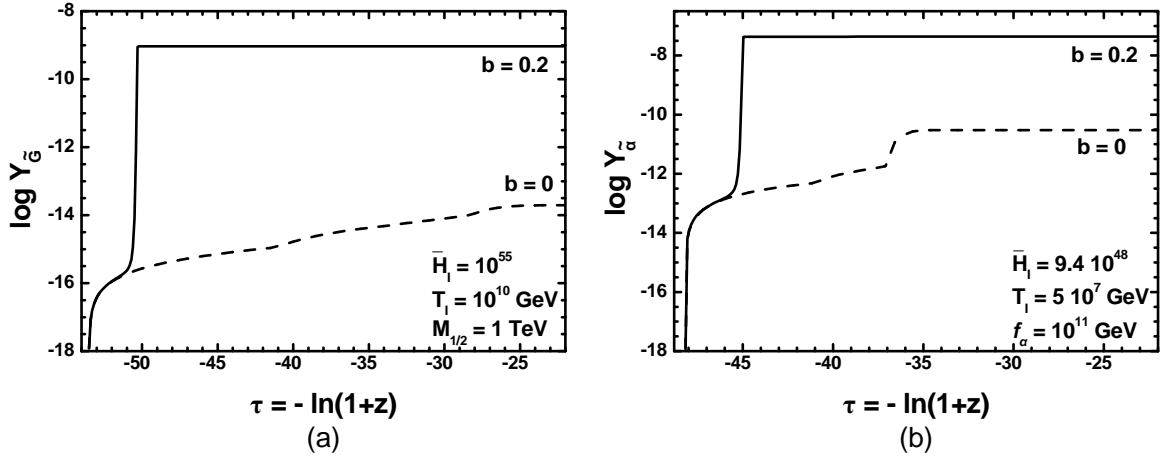


**FIGURE 3:** The evolution of the logarithm of the  $X$  yield,  $Y_X$  with  $X = \tilde{G}$  [ $X = \tilde{a}$ ] as a function of  $\tau$  (a) [(b)] for  $a = 0.5$ ,  $T_1 = 10^{10}$  GeV [ $T_1 = 5 \cdot 10^7$  GeV],  $\bar{H}_1 = 10^{55}$  [ $\bar{H}_1 = 9.4 \cdot 10^{48}$ ],  $M_{1/2} = 1$  TeV [ $f_a = 10^{11}$  GeV] and  $b = 0$  (dashed line) or  $b = 0.2$  (solid line). We obtain  $\Omega_X h^2 = 0.11$  for  $b = 0.2$  and  $m_{\tilde{G}} = 0.44$  GeV [ $m_{\tilde{a}} = 9.5$  MeV].

In Fig. 3-(a) [Fig. 3-(b)] we observe that for  $b = 0$ , where a pure KD era occurs,  $Y_X$  with  $X = \tilde{G}$  [ $X = \tilde{a}$ ] takes its final value, more or less, close to the onset of the RD era for  $\tau_{\text{KR}} \simeq -28.5$  [ $\tau_{\text{KR}} \simeq -25.4$ ] – corresponding to  $T_{\text{KR}} \simeq 0.23$  [ $T_{\text{KR}} \simeq 0.017$ ] –, according to the well-known results of Ref. [32]. Namely, for  $X = \tilde{G}$  the resulting  $Y_{X0}$  (for  $b = 0$ ) is not so precise, since the used  $C_X^{\text{HT}}$  from Eq. (3.3) gives reliable results mainly for  $T \gg T_C$ . On the other hand, for  $X = \tilde{a}$  (and  $b = 0$ ),  $Y_X$  is calculated employing for  $T < T_{\text{SUSY}}$ ,  $C_{\tilde{a}} = C_{\tilde{a}}^{\text{LT}}$  obtained from the non-relativistic formalism of Ref. [32] with the  $m_i$ 's indicated in Eq. (3.4). Due to the Boltzmann suppression occurred for  $T < T_{\text{SUSY}}$ ,  $Y_X$  takes its present value at about  $T \simeq T_{\text{SUSY}}$  ( $\tau_{\text{SUSY}} = -37$ ). On the contrary, for  $b = 0.2$  and the inputs of Fig. 3-(a) [Fig. 3-(b)],  $Y_X$  takes its final value at  $\tau \simeq -50$  [ $\tau \simeq -45$ ] where  $q$  develops its first – for  $k = 0$  in Eq. (2.20) – extremum. Obviously,  $Y_{X0}$  for  $b = 0.2$  is much larger than its value for  $b = 0$  but still lower than its value in the SC for  $T \simeq T_1$ . Indeed, for the inputs of Fig. 3-(a) [Fig. 3-(b)] we obtain  $\log Y_{\tilde{G}0} = -5.3$  [ $\log Y_{\tilde{a}0} = -3.94$ ] in the SC.

Despite the fact that  $C_X^{\text{HT}}$  in Eq. (3.9) has a rather simple form given by Eq. (3.3), it is not straightforward to find a general analytical result for the integration of Eq. (3.9). This is mainly due to the fact that the integrand includes  $g_q$  and  $g_b$  which depend on the  $q$  and  $Q$  evolution in a rather complicate way. Nevertheless, we can write simple empirical relations which reproduce rather accurately (within 5%) our numerical results for  $X = \tilde{G}$  [ $X = \tilde{a}$ ],  $a = 0.5$ ,  $b = 0.2$ ,  $T_1 = 10^{10}$  GeV or  $T_1 = 10^9$  GeV [ $T_1 = 10^9$  GeV or  $T_1 = 5 \cdot 10^7$  GeV]. Namely

$$\Omega_X h^2 = \left[ \left( a_{1X} \log \frac{T_1}{\text{GeV}} + b_{1X} \right) \log \bar{H}_1 + \left( a_{2X} \log \frac{T_1}{\text{GeV}} + b_{2X} \right) \right] \begin{cases} M_1^2 / m_{\text{P}} m_X & \text{for } X = \tilde{G}, \\ m_{\text{P}} m_X / f_a^2 & \text{for } X = \tilde{a}, \end{cases} \quad (3.15)$$

where the numerical coefficients  $a_{1X}$ ,  $a_{2X}$ ,  $b_{1X}$ ,  $b_{2X}$  are given by

$$(a_{1X}, a_{2X}, b_{1X}, b_{2X}) = \begin{cases} (-1.603, 95.26, 1.4223, -845.78) \cdot 10^{11} & \text{for } X = \tilde{G}, \\ (-1.2505, 71.064, 9.5244, -541.6) \cdot 10^5 & \text{for } X = \tilde{a}. \end{cases}$$

We, thus, conclude that in our QS, for a naturally expected hierarchy among  $T_1$ ,  $T_C$  and  $T_{\text{KR}}$ , the calculation of  $\Omega_X h^2$  depends exclusively on  $C_X^{\text{HT}}$  and not on  $C_X^{\text{LT}}$ ,  $\Gamma_i$ 's and  $m_i$ 's.

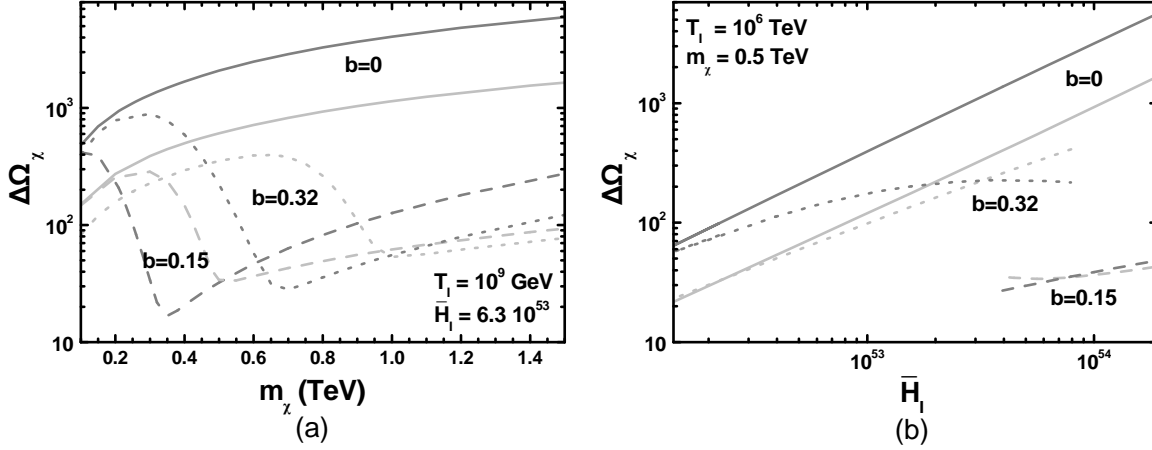


**FIGURE 4:**  $\Delta\Omega_\chi$  versus (a)  $m_\chi$  for  $\bar{H}_I = 1.6 \cdot 10^{53}$  and (b)  $\bar{H}_I$  for  $m_\chi = 0.5$  TeV. In both cases we take  $a = 0.5$ ,  $T_I = 10^9$  GeV (or  $\tau_I = -51.16$ ),  $\langle\sigma v\rangle = 10^{-8}$  GeV $^{-2}$  [ $\langle\sigma v\rangle = 10^{-10}x$  GeV $^{-2}$ ] (light gray [gray] lines) and  $b = 0$  (solid lines),  $b = 0.15$  (dashed lines) and  $b = 0.32$  (dotted lines).

#### 4. CDM FROM THERMAL PRODUCTION OF WIMPS

Employing the formalism developed in the previous section, we can analyze the behavior of  $\Omega_\chi h^2$  as a function of the free parameters of the QS (Sec. 4.1) and construct regions allowed by the various constraints (Sec. 4.2).

##### 4.1 THE ENHANCEMENT OF $\Omega_\chi h^2$

The presence of  $g_q > 1$  in Eq. (3.12) and, mainly, in Eq. (3.14) reduces  $J_F$ , thereby increasing  $\Omega_\chi h^2$  w.r.t its value,  $\Omega_\chi h^2|_{SC}$ , in the SC – i.e., setting  $g_q = g_b = 1$  in Eq. (3.9). The resulting enhancement can be estimated, by defining the quantity:

$$\Delta\Omega_\chi = \frac{\Omega_\chi h^2 - \Omega_\chi h^2|_{SC}}{\Omega_\chi h^2|_{SC}}. \quad (4.1)$$

The behavior as a function of our free parameters of  $\Delta\Omega_\chi$  within our QS can be inferred from Fig. 4 where we display  $\Delta\Omega_\chi$  versus  $m_\chi$  – see Fig. 4-(a) – for  $\bar{H}_I = 6.3 \cdot 10^{53}$  or  $\bar{H}_I$  – see Fig. 4-(b) – for  $m_\chi = 0.5$  TeV. We isolate two cases commonly encountered in the analysis of several models, fixing  $\langle\sigma v\rangle = 10^{-8}$  GeV $^{-2}$  (light gray curves) and  $\langle\sigma v\rangle = 10^{-10}x$  GeV $^{-2}$  (gray curves). We take  $b = 0$  (solid lines),  $b = 0.15$  (dashed lines) and  $b = 0.32$  (dotted lines). The chosen  $\bar{H}_I$  results to  $\Omega_q^{BBN} \simeq 0.01$ , 0.068 or 0.19 for  $b = 0, 0.15$  or 0.32 correspondingly, whereas in Fig. 4-(b)  $\Omega_q^{BBN}$  ranges from  $5 \cdot 10^{-6}$  to 0.079 for  $b = 0$  or from 0.05 to 0.21 [from 0.016 to 0.21] for  $b = 0.15$  [ $b = 0.32$ ]. Due to the band structure of the allowed parameter space of the model – see Fig. 2-(a) – not all  $\Omega_q^{BBN}$ 's are achievable for any  $b$ .

Clearly, for  $b = 0$  we get a pure KD era and our results reduce to those presented in Ref. [26], i.e.,  $\Delta\Omega_\chi$  increases when  $m_\chi$  or  $\bar{H}_I$  (and consequently  $\Omega_q^{BBN}$ ) increases or when  $\langle\sigma v\rangle$  decreases – see Fig. 4-(a) and (b). On the contrary, for  $b \neq 0$ ,  $\Delta\Omega_\chi$  depends crucially on the hierarchy between  $\tau_F$  and  $\tau_{ext}$ . Given that  $J_F$  takes its main contribution from  $g_q$  for  $\tau \sim \tau_F$ ,  $J_F$  is enhanced – see Eq. (3.14) – if  $\tau_F$  is lower than  $\tau_{ext}$  and close to it, since  $g_q$  is suppressed ( $g_q \simeq 1$ ) for  $\tau \simeq \tau_{ext}$ . As a consequence – see Eqs. (3.8) and (3.14) –  $\Delta\Omega_\chi$  diminishes. This argument is highlighted



$\langle\sigma v\rangle$ (GeV $^{-2}$ )	$-\tau_F$	$b = 0.15, \tau_{\text{ext}} \approx -33.1$			$b = 0.32, \tau_{\text{ext}} \approx -33.8$		
		$\Delta\Omega_\chi _{\text{min}}$	$\tau_F^{\text{min}}$	$m_\chi^{\text{min}}/\text{TeV}$	$\Delta\Omega_\chi _{\text{min}}$	$\tau_F^{\text{min}}$	$m_\chi^{\text{min}}/\text{TeV}$
$10^{-8}$	31.8 – 34.6	32.6	–33.4	0.52	53.2	–34.15	1.01
$10^{-10}_x$	32.3 – 35.2	16.8	–33.5	0.35	28	–34.3	0.69

TABLE 1: The minima of  $\Delta\Omega_\chi$ ,  $\Delta\Omega_\chi|_{\text{min}}$ , occurring at the freeze-out logarithmic time  $\tau_F^{\text{min}}$  or the mass of  $\chi$   $m_\chi^{\text{min}}$ , for  $a = 0.5$ ,  $T_I = 10^9$  GeV,  $\bar{H}_I = 6.3 \cdot 10^{53}$  and several  $\langle\sigma v\rangle$ 's and  $b$ 's employed in Fig. 4-(a). We also show the range of  $\tau_F$  for  $0.1 \leq m_\chi/\text{TeV} \leq 1.5$  and the logarithmic time  $\tau_{\text{ext}}$  at which the closest to  $\tau_F$  peak in the  $q$ -evolution takes place.

by Table 1. There, we list the range of  $\tau_F$  for  $0.1 \leq m_\chi/\text{TeV} \leq 1.5$  and  $\langle\sigma v\rangle = 10^{-8}$  GeV $^{-2}$  or  $\langle\sigma v\rangle = 10^{-10}_x$  GeV $^{-2}$  and the logarithmic time  $\tau_{\text{ext}}$  at which the closest to  $\tau_F$ 's peak in the  $q$ -evolution takes place for  $b = 0.15$  or  $b = 0.32$  and  $\bar{H}_I = 6.3 \cdot 10^{53}$ . Clearly,  $\tau_F$  [ $\tau_{\text{ext}}$ ] is independent of  $b$  or  $\bar{H}_I$  [ $m_\chi$  or  $\langle\sigma v\rangle$ ]. As  $\tau_F$  moves closer to  $\tau_{\text{ext}}$ ,  $\Delta\Omega_\chi$  decreases with its minimum  $\Delta\Omega_\chi|_{\text{min}}$  occurring at  $\tau_F \approx \tau_F^{\text{min}}$  or  $m_\chi = m_\chi^{\text{min}}$ . Note that  $\tau_F^{\text{min}}$  does not coincide with  $\tau_{\text{ext}}$  always due to the presence of  $Y_F$  in Eq. (3.14). The appearance of minima can be avoided if  $\tau_F$ 's happen to remain constantly lower than  $\tau_{\text{ext}}$ 's.

Increasing  $\bar{H}_I$  for fixed  $m_\chi = 0.5$  TeV leads to an increase of  $\Omega_q^{\text{BBN}}$  for the parameters of Fig. 2-(b). However, the expected increase of  $\Delta\Omega_\chi$  is less effective for  $\langle\sigma v\rangle = 10^{-10}_x$  GeV $^{-2}$  than for  $\langle\sigma v\rangle = 10^{-8}$  GeV $^{-2}$  as shown in Fig. 2-(b). Let us check, e.g., the case for  $b = 0.32$ . As  $\bar{H}_I$  increases in the first allowed band, shown in Fig. 2-(a), from 52.2 to 53.9,  $\tau_{\text{ext}}$  moves from  $-34$  to  $-33.8$  and influences  $\Delta\Omega_\chi$  for  $\langle\sigma v\rangle = 10^{-10}_x$  GeV $^{-2}$  more than for  $\langle\sigma v\rangle = 10^{-8}$  GeV $^{-2}$ . This is, because for  $\langle\sigma v\rangle = 10^{-10}_x$  GeV $^{-2}$ , we get  $\tau_F \approx -33.7$  which is closer to  $\tau_{\text{ext}}$ 's than  $\tau_F \approx -33.1$  which is taken for  $\langle\sigma v\rangle = 10^{-8}$  GeV $^{-2}$ . Variation of  $T_I$  (or equivalently  $\tau_I$ ) leads to a displacement of  $\tau_{\text{ext}}$ 's – see Eq. (2.20) – and therefore the minima of  $\Delta\Omega_\chi$  in Fig. 2-(a) or the limits of the non solid lines in Fig. 2-(b) are relocated. However, our results on the behavior of  $\Delta\Omega_\chi$  remain intact.

## 4.2 RESTRICTIONS IN THE $m_\chi - \langle\sigma v\rangle$ PLANE

Though the post-freeze-out  $Y_\chi$  in Eq. (3.14) stays essentially unchanged, residual annihilations of  $\chi$ 's occur up to the present, with several cosmological consequences. Recently, tight upper bounds on  $\langle\sigma v\rangle$ 's have been reported. These, however, depend on the identity of the products of the annihilation of  $\chi$ 's. To get a feeling of the relevant effects, we adopt the most restrictive bound which arises for the annihilation mode of  $\chi$ 's to  $e^+e^-$ . In particular, the constraints from BBN [51] and cosmic microwave background [52] result to the following bounds, respectively:

$$(a) \langle\sigma v\rangle \leq 3 \cdot 10^{-5} \text{ GeV}^{-2} \frac{m_\chi}{1 \text{ TeV}} \quad \text{and} \quad (b) \langle\sigma v\rangle \leq 4.4 \cdot 10^{-7} \text{ GeV}^{-2} \frac{m_\chi}{1 \text{ TeV}}. \quad (4.2)$$

Obviously the constraint of Eq. (4.2b) is much more restrictive than this from Eq. (4.2a). To be in harmony with the assumptions considered in the derivation of the above bounds, we consider hereafter  $\langle\sigma v\rangle$ 's independent of  $T$ .

Having fixed the parameters which determine the QS, we can derive restrictions on the parameters involved in the  $\Omega_\chi h^2$  calculation. This is done in Fig. 5 where we show the allowed parameter space in the  $m_\chi - \langle\sigma v\rangle$  plane for  $a = 0.5$  and  $T_I = 10^9$  GeV. We also take  $b = 0$  and  $\bar{H}_I = 6.3 \cdot 10^{53}$  or  $6.2 \cdot 10^{52}$  resulting to  $\Omega_q^{\text{BBN}} = 0.01$  or  $10^{-4}$  respectively in Fig. 5-(a),  $\bar{H}_I = 6.3 \cdot 10^{53}$  and  $b = 0.15$  or  $\bar{H}_I = 6.2 \cdot 10^{52}$  and  $b = 0.32$  yielding  $\Omega_q^{\text{BBN}} = 0.068$  or  $0.065$  respectively, in Fig. 5-(b).

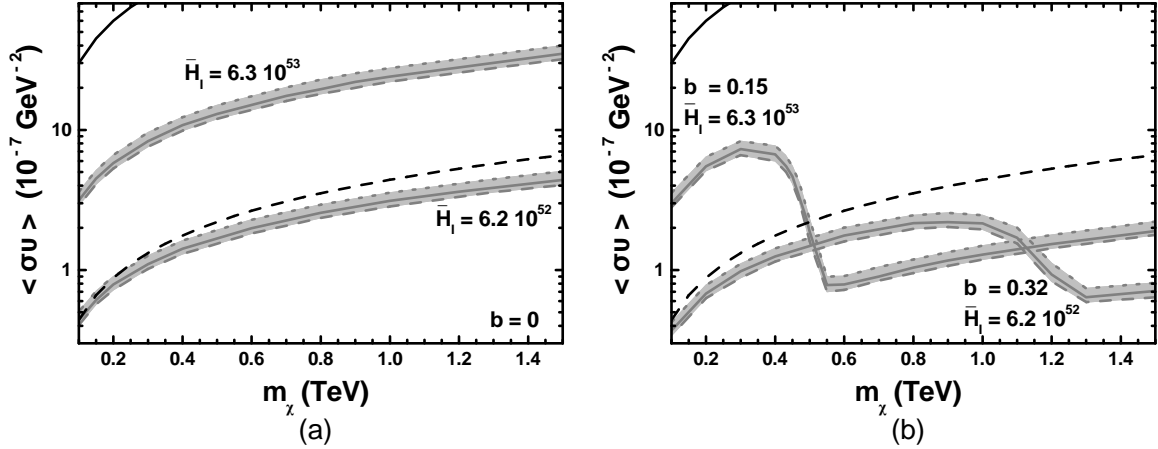


FIGURE 5: Restrictions in the  $m_\chi - \langle\sigma v\rangle$  plane for  $a = 0.5$ ,  $T_I = 10^9$  GeV and several  $b$ 's and  $\bar{H}_I$ 's indicated in the graphs (a) and (b). The light gray shaded areas are allowed by Eq. (1.2) whereas the region above the black solid [dashed] line is ruled out by the upper bound on  $\langle\sigma v\rangle$  from Eq. (4.2a) [Eq. (4.2b)] assuming  $\chi\chi \rightarrow e^+e^-$ . The conventions adopted for the residual lines are also shown.

$-\cdot-\cdot-\cdot-$   $\Omega_\chi h^2 = 0.097$   
 $-$   $\Omega_\chi h^2 = 0.11$   
 $- - -$   $\Omega_\chi h^2 = 0.12$

In the plots of Fig. 5 the upper bounds from Eq. (4.2a) and Eq. (4.2b) are denoted by black solid (left corner of each plot) and dashed lines respectively. On the other hand, the light gray shaded regions are confronted with Eq. (1.2). The gray dashed [dotted] lines correspond to the upper [lower] bound on  $\Omega_\chi h^2$  in Eq. (1.2), whereas the gray solid lines are obtained by fixing  $\Omega_\chi h^2$  to its central value in Eq. (1.2). We observe that  $\Omega_\chi h^2$  decreases as  $\langle\sigma v\rangle$  increases. This is due to the fact that  $\Omega_\chi h^2 \propto 1/\langle\sigma v\rangle$ , as can be deduced from Eqs. (3.8) and (3.14). We also observe that for  $\tau_F$  far away from  $\tau_{\text{ext}}$  the region allowed by Eq. (1.2) for  $b \neq 0$  reaches the one for  $b = 0$  with the same  $\bar{H}_I$ . However, when  $\tau_F$  reaches  $\tau_{\text{ext}}$ ,  $\Omega_\chi h^2$  decreases – as we explain in Sec. 4 – and therefore, the required for obtaining  $\Omega_\chi h^2$  in the range of Eq. (1.2)  $\langle\sigma v\rangle$  decreases too. As a consequence, although the allowed by Eq. (1.2) area in Fig. 5-(b) with  $b = 0.15$  approaches the corresponding area in Fig. 5-(a) with the same  $\bar{H}_I$  and violates the bound of Eq. (4.2b) for low  $m_\chi$ 's, it becomes compatible with the latter constraint for larger  $m_\chi$ 's.

We observe that, due to the dependence of  $\Omega_\chi h^2$  on the hierarchy between  $\tau_F$  and  $\tau_{\text{ext}}$  for  $b \neq 0$  we can achieve compatibility of the CDM constraint with the bounds of Eq. (4.2b) even for large  $\Omega_q^{\text{BBN}}$ . On the contrary, this can be attained for  $b = 0$  only tuning  $\Omega_q^{\text{BBN}} \lesssim 10^{-4}$ . However in both cases ( $b = 0$  and  $b \neq 0$ ) agreement with the requirement of Eq. (1.2a) implies almost two-three orders of magnitude higher  $\langle\sigma v\rangle$ 's than those required in the SC – c.f. Ref. [26]. It is worth mentioning that the obtained  $\langle\sigma v\rangle$ 's can assist us to interpret [55], through WIMP annihilation in the galaxy the reported excess on the positron and/or electron cosmic-ray flux [56], without invoking any pole effect [57], ad-hoc boost factor [58] or other astrophysical sources [59]. According to preliminary results [60], the best fits to the experimental data can be achieved for the annihilation channel  $\chi\chi \rightarrow \mu^+\mu^-$  with  $m_\chi \simeq (1 - 1.6)$  TeV and  $\langle\sigma v\rangle \simeq (1 - 5) \cdot 10^{-6}$  GeV $^{-2}$ . However, these values remain tightly restricted by the CMB constraint [52].

## 5. CDM FROM THERMAL PRODUCTION OF $e$ -WIMPs

Similarly to the previous section, we analyze the behavior of  $\Omega_\chi h^2$  as a function of the free parameters (Sec. 5.1), and we identify the parametric regions allowed by the various constraints (Sec. 5.2).

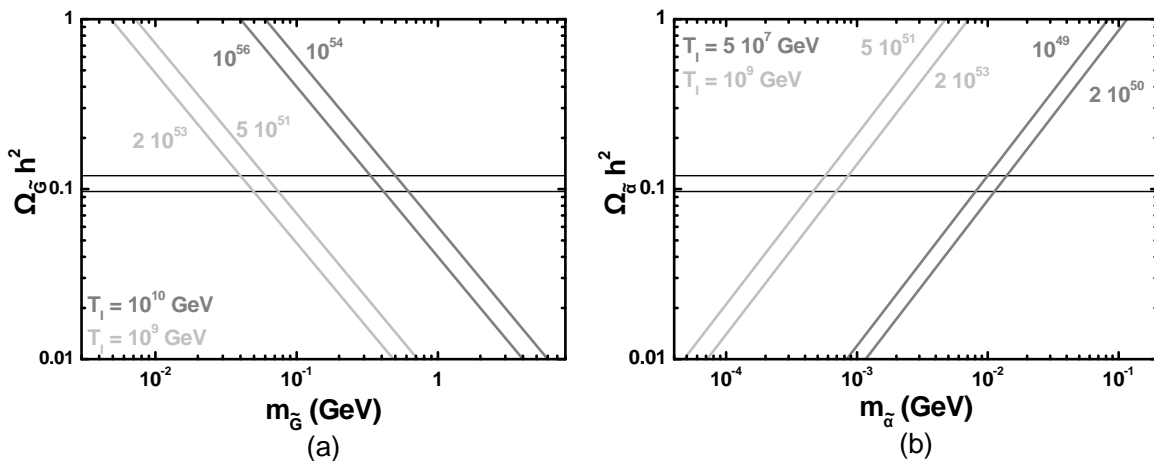


**FIGURE 6:**  $\Omega_X h^2$  as a function of  $m_X$  ( $X = \tilde{G}$  [ $X = \tilde{a}$ ]) for various  $\tilde{H}_1$ 's, indicated in the curves,  $a = 0.5$ ,  $b = 0.2$  and  $M_{1/2} = 1$  TeV [ $f_a = 10^{11}$  GeV] (a [b]). We set (a)  $T_I = 10^9$  GeV (light gray lines) or  $T_I = 10^{10}$  GeV (gray lines) and (b)  $T_I = 10^9$  GeV (light gray lines) or  $T_I = 5 \cdot 10^7$  GeV (gray lines). The CDM bounds of Eq. (1.2) are, also, depicted by the two thin lines.

As emphasized in Sec. 3.3.2, we focus on large  $T_I$ 's which are frequently met in the well-motivated models of SUSY inflation (see, e.g., Ref. [50]).

### 5.1 $\Omega_X h^2$ AS A FUNCTION OF THE FREE PARAMETERS

By varying the free parameters, useful conclusions can be drawn for the behavior of  $\Omega_X h^2$ . The results are presented in Fig. 6-(a) [Fig. 6-(b)] where we plot  $\Omega_X h^2$  as a function of  $m_X$  (with  $X = \tilde{G}$  [ $X = \tilde{a}$ ]) for  $a = 0.5$ ,  $b = 0.2$  and  $M_{1/2} = 1$  TeV [ $f_a = 10^{11}$  GeV],  $T_I = 10^9$  GeV (light gray lines),  $T_I = 10^{10}$  GeV (gray lines) [ $T_I = 10^9$  GeV (light gray lines) and  $T_I = 5 \cdot 10^7$  GeV (gray lines)]. We use various values for the  $\tilde{H}_1$ , indicated in the curves. The CDM bounds of Eq. (1.2) are, also depicted by the two thin lines. The results are derived numerically, but they can also be reproduced from the empirical expressions in Eq. (3.15).

For each choice of  $T_I$  in Fig. 6, the selected  $\tilde{H}_1$ 's belong to the allowed region of Fig. 2-(b) and yield  $\Omega_q^{\text{BBN}} > 10^{-5}$ . In all cases  $\Omega_X h^2$  is stabilized at  $T \gg T_C$  and therefore, its calculation exclusively depends on  $C_X^{\text{HT}}$  given by Eq. (3.3). For the  $T_I$ 's and  $\tilde{H}_1$ 's under consideration,  $\Omega_q^{\text{BBN}}$  and the  $\tau_{\text{ext}}$  closest to  $\tau_I$ , increase with  $\tilde{H}_1$ . Note that this fact is not explicitly shown in the approximate Eq. (2.20). As a consequence,  $\Omega_X h^2$  (which takes its present value close to this  $\tau_{\text{ext}}$ ) decreases as  $\tilde{H}_1$  increases. This feature is similar to what happens in the pure KD era – c.f. Ref. [32]. Similarly, we also observe  $\Omega_{\tilde{G}} h^2 \propto 1/m_{\tilde{G}}$ , whereas  $\Omega_{\tilde{a}} h^2 \propto m_{\tilde{a}}$  – see Eq. (3.15).

### 5.2 RESTRICTIONS IN THE $m_X - \log \tilde{H}_1$ PLANE

As already mentioned,  $X$  constitutes a good CDM candidate if  $\Omega_X h^2$  satisfies the criterion of Eq. (1.2). Enforcing the latter constraint we can derive restrictions in the  $m_X - \log \tilde{H}_1$  plane. We focus on  $(T_I, \tilde{H}_1)$ 's that belong in the first allowed band – depicted in Fig. 2-(b) – of our QS. For the sake of comparison, we present results even for  $b = 0$ , although the tracking behavior of our QS is not attained in this case as explained in Sec. 2.3.

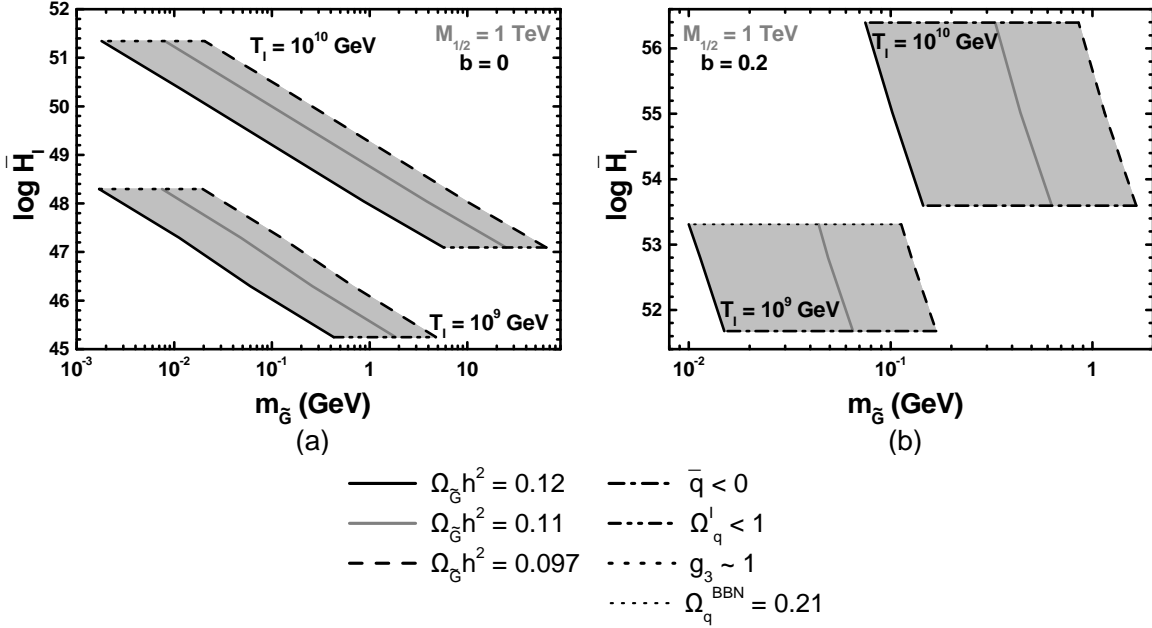


FIGURE 7: Allowed (lightly gray shaded) regions in the  $m_{\tilde{G}} - \log \bar{H}_I$  plane for  $\tilde{G}$  CDM with  $0.5 \leq M_{1/2}/\text{TeV} \leq 1.5$ ,  $a = 0.5$ ,  $T_I = 10^{10}$  GeV or  $T_I = 10^9$  GeV and (a)  $b = 0$  and (b)  $b = 0.2$ . The conventions adopted for the various lines are also shown.

**5.2.1 GRAVITINO COLD DARK MATTER.** We recall that the free parameters in the present case are:  $m_{\tilde{G}}$ ,  $T_I$ ,  $M_{1/2}$  and  $\bar{H}_I$  with fixed  $b$  and  $a = 0.5$ .

In Fig. 7-(a) [Fig. 7-(b)] we plot the allowed (lightly gray shaded) regions in the  $m_{\tilde{G}} - \bar{H}_I$  plane, letting  $M_{1/2}$  vary in the interval  $(0.5 - 1.5)$  TeV, for  $a = 0.5$ ,  $b = 0$  [ $b = 0.2$ ] and  $T_I = 10^9$  GeV or  $10^{10}$  GeV. The black solid [dashed] lines correspond to the upper [lower] bound on  $\Omega_{\tilde{G}} h^2$  in Eq. (1.2a), whereas the gray solid lines have been obtained by fixing  $\Omega_{\tilde{G}} h^2$  to its central value in Eq. (1.2a) for  $M_{1/2} = 1$  TeV. Having in mind Eq. (3.15), we construct the solid [dashed] line for  $M_{1/2} = 0.5$  TeV [ $M_{1/2} = 1.5$  TeV].

The upper [lower] boundary curve (dotted [double dot-dashed] line) of the allowed regions in Fig. 7-(a) arises from the saturation of  $g_3 < 1$  [Eq. (2.13)]. Recall that  $g_3 < 1$  allows employing  $C_{\tilde{G}} = C_{\tilde{G}}^{\text{HT}}$  self consistently in our calculation. On the other hand, in Fig. 7-(b), the upper and lower boundaries (dashed lines) of the allowed area for  $T_I = 10^{10}$  GeV arise from the band structure of our QS. This is, also, the origin of the lower boundary (dashed line) of the allowed area for  $T_I = 10^9$  GeV. The upper boundary (thin dotted line) of this area comes from Eq. (2.14). We observe that the required  $m_{\tilde{G}}$ 's increase with  $T_I$  as expected from Eq. (3.15).

As emphasized in Ref. [32], for  $b = 0$ , acceptable  $\Omega_{\tilde{G}} h^2$ 's require a fine tuning of  $\Omega_q^{\text{BBN}}$ 's to very low values. Indeed, in the allowed regions of Fig. 7-(a) for  $T_I = 10^9$  GeV [ $T_I = 10^{10}$  GeV] we have  $10^{-19} \lesssim \Omega_q^{\text{BBN}} \lesssim 10^{-13}$  [ $10^{-21} \lesssim \Omega_q^{\text{BBN}} \lesssim 10^{-13}$ ]. Such an unattractive tuning is not needed for  $b = 0.2$ . In fact, in the allowed regions of Fig. 7-(b) for  $T_I = 10^9$  GeV [ $T_I = 10^{10}$  GeV] we have  $10^{-4} \lesssim \Omega_q^{\text{BBN}} \lesssim 0.21$  [ $10^{-6} \lesssim \Omega_q^{\text{BBN}} \lesssim 0.064$ ]. We conclude, therefore, that  $\tilde{G}$  is a natural CDM candidate within our QS.

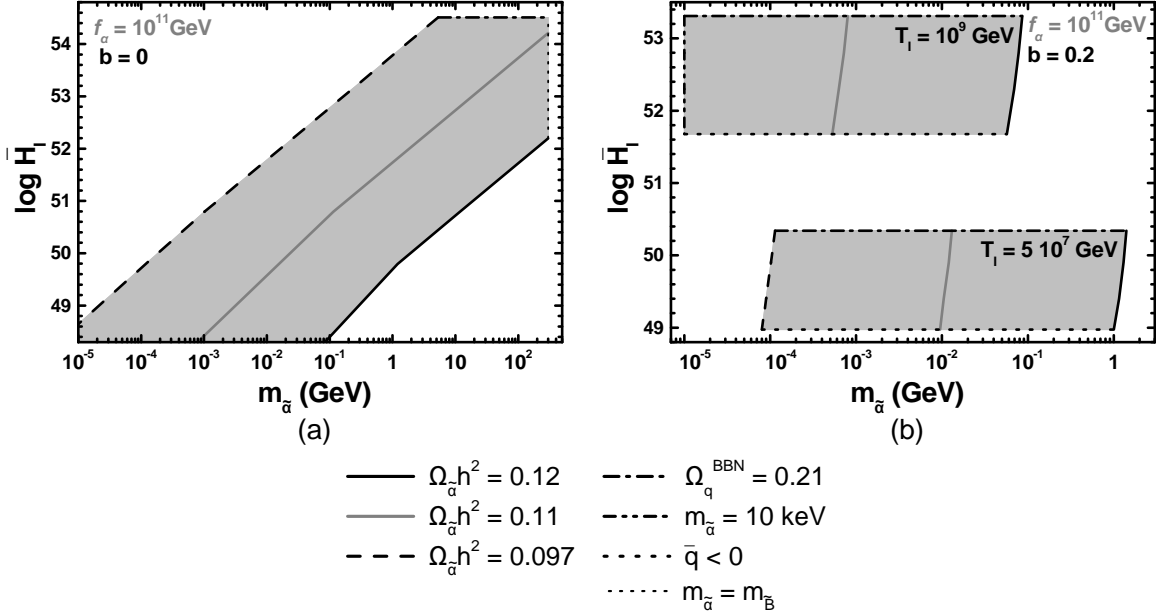


FIGURE 8: Allowed (lightly gray shaded) regions in the  $m_{\tilde{a}} - \log \bar{H}_I$  plane for  $\tilde{a}$  CDM,  $10^{10} \leq f_a/\text{GeV} \leq 10^{12}$ ,  $a = 0.5$ ,  $T_1 = 10^9 \text{ GeV}$  or  $T_1 = 5 \cdot 10^7 \text{ GeV}$  and (a)  $b = 0$  or (b)  $b = 0.2$ . For  $b = 0$  we use the  $m_i$ 's shown in Eq. (3.4). The conventions adopted for the various lines are also shown.

5.2.2 AXINO COLD DARK MATTER. In considering the candidature of  $\tilde{a}$  for the major CDM component of the universe, we have initially to assume that the scalar SUSY partner of  $\tilde{a}$  (known as saxion) does not decay [13] out-of-equilibrium producing entropy and thereby, diluting  $\Omega_{\tilde{a}} h^2$ . We then have to ensure the consistency of the hypothesis that  $\tilde{a}$  decouples from the thermal bath at a temperature  $T_D > T_1$ . To this end, we check that for every  $T < T_1$  the following condition is valid:

$$H(T) > \Gamma_{\tilde{a}}(T) \quad \text{where} \quad \Gamma_{\tilde{a}} \sim 6 N_F (N_3^2 - 1) g_a^2 g_3^2 n^{\text{eq}} / 2. \quad (5.1)$$

Here,  $\Gamma_{\tilde{a}}$  is the interaction rate of  $\tilde{a}$ 's with the thermal bath [54],  $N_F = 12$  and  $N_3 = 3$  [32]. The free parameters in the present case are:  $m_{\tilde{a}}$ ,  $f_a$ ,  $T_1$  and  $\bar{H}_I$  with fixed  $b$  and  $a = 0.5$ .

In Fig. 8-(a) [Fig. 8-(b)] we display the allowed (lightly gray shaded) regions in the  $m_{\tilde{a}} - \bar{H}_I$  plane for  $10^{10} \leq f_a/\text{GeV} \leq 10^{12}$ ,  $a = 0.5$ ,  $b = 0$  [ $b = 0.2$ ] and  $T_1 = 10^9 \text{ GeV}$  or  $T_1 = 5 \cdot 10^7 \text{ GeV}$ . The black solid [dashed] lines correspond to the upper [lower] bound on  $\Omega_{\tilde{a}} h^2$  in Eq. (1.2a), whereas the gray solid lines have been obtained by fixing  $\Omega_{\tilde{a}} h^2$  to its central value in Eq. (1.2a) for  $f_a = 10^{11} \text{ GeV}$ . In practice, the solid [dashed] line is constructed for  $f_a = 10^{12} \text{ GeV}$  [ $f_a = 10^{10} \text{ GeV}$ ]. This can be understood taking into account the empirical relations for  $\Omega_{\tilde{a}} h^2$  given in Ref. [32] [Eq. (3.15)] for  $b = 0$  [ $b = 0.2$ ].

The upper boundary curves (dot-dashed line) of the allowed areas in Fig. 8 come from the upper bound on  $\Omega_q^{\text{BBN}}$  in Eq. (2.14). The right boundary (thin line) of the allowed area in Fig. 8-(a) arises from the upper bound of Eq. (1.2b) assuming that  $\tilde{B}$  is the NLSP, with a mass as in Eq. (3.4). Needless to say that this upper bound can be modified if there is another SUSY particle lighter than  $\tilde{B}$ . The relevant area terminates from below at  $T_{\text{KR}} \simeq 1 \text{ TeV}$ , so that our formulas for  $C_{\tilde{a}}^{\text{LT}}$  in Ref. [32] are fully applicable. The low boundary curves of the allowed areas in Fig. 8-(b) arise from the band structure of the parameter space of the QS under study.

Contrary to the case of  $\widetilde{G}$ , we observe that the required  $m_{\tilde{a}}$ 's increase when  $T_1$  decreases, as expected from Eq. (3.15). In the allowed region of Fig. 8-(a) we get  $10^{-13} \lesssim \Omega_q^{\text{BBN}} \lesssim 0.21$ . In this case (with  $b = 0$ ), the  $\Omega_{\tilde{a}}h^2$  calculation is realized employing  $C_{\tilde{a}}^{\text{LT}}$  corresponding to the  $m_i$ 's indicated in Eq. (3.4). As outlined in Ref. [32] and deduced from Fig. 3-(b), the  $\Omega_{\tilde{a}}h^2$  calculation in this regime – and therefore, the allowed area of Fig. 8-(a) – is independent of  $T_1$ , provided  $T_1 > T_{\text{SUSY}}$ . On the other hand, in the allowed regions of Fig. 8-(b) for  $T_1 = 10^9$  GeV [ $T_1 = 5 \cdot 10^7$  GeV] (and  $b = 0.2$ ), we have  $10^{-4} \lesssim \Omega_q^{\text{BBN}} \lesssim 0.21$  [ $0.031 \lesssim \Omega_q^{\text{BBN}} \lesssim 0.21$ ] and the  $\Omega_{\tilde{a}}h^2$  calculation depends exclusively on  $C_{\tilde{a}}^{\text{HT}}$ , as underlined in Sec. 3.3.2. Larger  $m_{\tilde{a}}$ 's are allowed in the case of Fig. 8-(a). Obviously, in both cases  $\tilde{a}$  turns out to be a natural CDM candidate for a wide range of  $m_{\tilde{a}}$ 's. However, within our QS ( $b > 0$ ), this result is insensitive to the low energy s-particle spectrum of the theory but depends on  $T_1$ .

## 6. CONCLUSIONS

We studied a quintessential model based on an inverse-power-law potential supplemented with a Hubble-induced mass term for the quintessence field,  $q$  – see Eq. (2.1). We verified that this term ensures the presence of a period dominated by the kinetic energy of  $q$  and allows the quintessential energy density to develop a tracker behavior sufficiently early, alleviating in this way the coincidence problem. In addition to the numerical treatment of the relevant equations (which is mandatory in order to obtain a reliable description of the quintessential dynamics) we presented a qualitative but rather comprehensive semi-analytical approach. The parameters of the model ( $a, b, T_1, \bar{H}_1$ ) were confined so as  $\Omega_q(T_1) = 1$  and were constrained by current observational data originating from BBN, the present acceleration of the universe, the inflationary scale and the DE density parameter.

We found that  $0 < a < 0.6$  and that there is a reasonably allowed region in the  $(b, \bar{H}_1)$  plane with  $b$  mildly tuned to values of order 0.1. Extrapolating the results of Ref. [39] to higher temperatures, we showed that, contrary to the pure KD era, the KD generated in this model is characterized by an oscillatory evolution of  $q$  and the barotropic index.

We then examined the impact of this modified KD epoch on the thermal abundance,  $\Omega_X h^2$ , of WIMPs and  $e$ -WIMPs. Solving the problem numerically and semi-analytically we found that:

- $\Omega_\chi h^2$ , with  $\chi$  a WIMP, increases w.r.t its value in the SC. Its increase is not monotonic as in the case of a pure KD era, but crucially depends on the hierarchy between the freeze-out temperature and the temperature where the evolution of  $q$  develops extrema.
- $\Omega_X h^2$  with  $X$  an  $e$ -WIMP (gravitino,  $\widetilde{G}$ , or axino,  $\tilde{a}$ ) takes its present value at the closest temperature to  $T_1$ , where  $q$  develops its extremum. As a consequence, while  $\Omega_X h^2$  decreases w.r.t its value in SC, it increases w.r.t its value in the pure KD phase, and both  $\widetilde{G}$  and  $\tilde{a}$  arise as natural CDM candidates for masses in the range  $(10^{-4} - 1)$  GeV.

We note that, additional BBN bounds might arise due to possible decays of the NLSP. Including these effects would have introduced significant model-dependence in our analysis, and would be relevant mainly for gravitinos, whose interactions are extremely suppressed. Even in this case the changes would be in at the numerical level, while the qualitative features of our discussion remain valid.

Given that we did not adopt a specific theoretical framework in our approach, we kept for simplicity and better definiteness  $b$  constant during the various phases of the  $q$  evolution – c.f. Ref. [39]. However, within supergravity,  $b$  may change from phase to phase – see, e.g., Ref. [61] –, thus affecting the quintessential dynamics – see Sec. 2.3. We checked that the value of  $b$  is to remain almost constant (at the level of  $\pm 10\%$ ) during the RD era which follows the KD era, for the tracker solution to be joined in time. On the contrary, if we switch off  $V_b$  after the onset of the matter domination, our results on  $\Omega_{q0}$  and  $w_q(0)$  remain more or less intact. Moreover,  $\Omega_X h^2$ , when  $X$  is a WIMP, increases [decreases] when  $b$  decreases [increases] after the KD era – see Eq. (3.14). On the other hand,  $\Omega_X h^2$ , if  $X$  is an  $e$ -WIMP, is not so sensitive to possible alterations of  $b$  during the post-kination phases, since its magnitude is determined mainly during the KD era.

Further work [60] is required in order to establish whether the enhancements of  $\Omega_X h^2$  obtained in our QS can explain the reported [56] results on the cosmic-ray fluxes through WIMP annihilation in the galaxy. In addition, it would be interesting to check whether the extrema in the evolution of  $q$  affect the interference between thermal leptogenesis and neutrino masses in conjunction with the  $\tilde{G}$  constraint – see, e.g., Ref. [62].

## ACKNOWLEDGMENTS

S.L and C.P have been supported by the FP6 Marie Curie Excellence grant MEXT-CT-2004-014297. SL also acknowledges support by the European Research and Training Network UniverseNet, MRTPN-CT-2006 035863-1.

## APPENDIX A

### TRACKING QUINTESSENCE AND THE $\tilde{G}$ CONSTRAINT

In this appendix, we analyze the implications of our quintessential scheme for the unstable  $\tilde{G}$ . In this case,  $\tilde{G}$  can decay after the onset of BBN, affecting the primordial abundances of the light elements in an unacceptable way. In order to avoid spoiling the success of BBN, an upper bound on  $Y_{\tilde{G}}$  is to be extracted as a function of  $m_{\tilde{G}}$  and the hadronic branching ratio of  $\tilde{G}$ ,  $B_h$  [63, 64, 65]. This is the well-known  $\tilde{G}$  constraint. In what follows, we specify some representative values of this constraint, taking into account the most up-to-date analysis of Ref. [63]. Note that we here review – c.f. Ref. [32] – the  $m_{\tilde{G}}$ 's which correspond to different  $Y_{\tilde{G}}(T_{\text{BBN}})$ 's, decoding more precisely the relevant figures. In particular, if  $\tilde{G}$  decays mainly to photon and photino, from Fig. 1 of Ref. [63] we can deduce:

$$Y_{\tilde{G}}(T_{\text{BBN}}) \lesssim \begin{cases} 10^{-15} \\ 10^{-14} \\ 10^{-13} \end{cases} \quad \text{for } m_{\tilde{G}} \simeq \begin{cases} 0.43 \text{ TeV} \\ 0.69 \text{ TeV} \\ 10.6 \text{ TeV} \end{cases} \quad \text{and } B_h = 0.001, \quad (\text{A.1})$$

whereas if  $\tilde{G}$  decays mainly to gluons and gluinos, from Fig. 2 of Ref. [63] we can deduce:

$$Y_{\tilde{G}}(T_{\text{BBN}}) \lesssim \begin{cases} 10^{-15} \\ 10^{-16} \\ 8.5 \cdot 10^{-15} \end{cases} \quad \text{for } m_{\tilde{G}} \simeq \begin{cases} 0.2 \text{ TeV} \\ 0.67 \text{ TeV} \\ 10 \text{ TeV} \end{cases} \quad \text{and } B_h = 1. \quad (\text{A.2})$$

$m_{\tilde{G}}$ (TeV)	$\bar{H}_1^{\min}$	$T_{\text{KR}}^{\max}$ (GeV)
$B_h = 0.001$		
0.43	$1.3 \cdot 10^{46}$	$1.1 \cdot 10^5$
0.69	$3.5 \cdot 10^{44}$	$3.9 \cdot 10^6$
10.6	$5 \cdot 10^{42}$	$2.7 \cdot 10^8$
$B_h = 1$		
0.2	$7.9 \cdot 10^{46}$	$2.5 \cdot 10^4$
0.67	$1.1 \cdot 10^{47}$	$1.7 \cdot 10^4$
10	$1.5 \cdot 10^{44}$	$8.7 \cdot 10^6$

$m_{\tilde{G}}$ (TeV)	$b = 0.15$		$b = 0.32$	
	$\bar{H}_1/10^{50}$			
	$3.9 \cdot 10^3$	$1.8 \cdot 10^4$	$1.7 \cdot 10^2$	$7.9 \cdot 10^3$
$Y_{\tilde{G}}/10^{-17}$				
0.43	8.7	7.6	22	15
0.69	4.6	4	12	8.2
10.6	1.96	1.7	5	3.6
0.2	33	29	85	59
0.67	4.7	4	12	8.7
10	1.96	1.7	5	3.6

(a)
(b)

**TABLE 2:** The minimum values of  $\bar{H}_1$ ,  $\bar{H}_1^{\min}$ , and the maximum values of  $T_{\text{KR}}$ ,  $T_{\text{KR}}^{\max}$ , dictated by the  $\tilde{G}$  constraint for  $b = 0$  and  $B_h = 0.001$  or  $1$  (a) and the obtained  $Y_{\tilde{G}}(T_{\text{BBN}})$  for  $b = 0.15$  and  $b = 0.32$  and the boundary values of  $\bar{H}_1$ 's of the first allowed band depicted in Fig. 2-(a) (b). We use various  $m_{\tilde{G}}$ 's indicated in the tables,  $a = 0.5$ ,  $T_1 = 10^9$  GeV and  $M_{1/2} = 1$  TeV.

In the SC (where no late-time entropy production is expected) Eqs. (A.1) and (A.2) imply stringent upper bounds on  $T_1$ , for fixed  $M_{1/2}$ . For the indicative value  $M_{1/2} = 1$  TeV, we find

$$T_1 \lesssim \begin{cases} 10^6 \text{ GeV} \\ 2.3 \cdot 10^7 \text{ GeV} \\ 5.6 \cdot 10^8 \text{ GeV} \end{cases} \text{ for } m_{\tilde{G}} \simeq \begin{cases} 0.43 \text{ TeV} \\ 0.69 \text{ TeV} \\ 10.6 \text{ TeV} \end{cases} \text{ and } B_h = 0.001, \text{ or} \quad (\text{A.3})$$

$$T_1 \lesssim \begin{cases} 1.45 \cdot 10^5 \text{ GeV} \\ 9 \cdot 10^4 \text{ GeV} \\ 4.8 \cdot 10^7 \text{ GeV} \end{cases} \text{ for } m_{\tilde{G}} \simeq \begin{cases} 0.2 \text{ TeV} \\ 0.67 \text{ TeV} \\ 10 \text{ TeV} \end{cases} \text{ and } B_h = 1. \quad (\text{A.4})$$

Clearly, the upper bound on  $T_1$  becomes significantly more restrictive for large  $B_h$ 's and low  $m_{\tilde{G}}$ 's. These restrictions on  $T_1$  can be avoided in both the pure kination scenario and our QS.

Indeed, in the case of a pure KD era the  $\tilde{G}$  constraint entails a lower bound on  $\bar{H}_1$ ,  $\bar{H}_1^{\min}$ , which can be transformed to an upper bound on  $T_{\text{KR}}$ ,  $T_{\text{KR}}^{\max}$ , for fixed  $T_1$ ,  $M_{1/2}$  and  $m_{\tilde{G}}$  – c.f. Ref. [32]. Setting  $T_1 = 10^9$  GeV and  $M_{1/2} = 1$  TeV, we present in Table 2-(a) the corresponding  $\bar{H}_1^{\min}$ 's and  $T_{\text{KR}}^{\max}$ 's for several  $m_{\tilde{G}}$ 's and  $B_h$ 's. Clearly, as the  $Y_{\tilde{G}}$ 's decrease, the required  $\bar{H}_1^{\min}$ 's [ $T_{\text{KR}}^{\max}$ 's] increase [decrease]. On the other hand, as we emphasized in Sec. 3.3.2,  $Y_{\tilde{G}}$  within our QS is stabilized close to the temperature  $T_{\text{exp}}(k = 0)$  which correspond to  $\tau_{\text{ext}}(k = 0)$  – see Eq. (2.20) – where the earliest peak of the  $q$  evolution occurs. Therefore, we expect that the  $\tilde{G}$  constraint imposes an upper bound on  $T_{\text{exp}}(k = 0)$ , which is a function of  $H_1$  and  $T_1$ . However, due to the band structure of the allowed parameter space of our QS, only certain  $\bar{H}_1$ 's are available for each  $b$  – see Fig. 2-(a). For this reason, we opt to present in Table 2-(b) the  $Y_{\tilde{G}}$ 's resulting on the boundaries of the first allowed band for  $b = 0.15$  and  $b = 0.32$  fixing again  $T_1 = 10^9$  GeV and  $M_{1/2} = 1$  TeV. For the selected  $\bar{H}_1$ 's we obtain  $T_{\text{ext}}(k = 0) \simeq 2.5 \cdot 10^7$  GeV [ $T_{\text{ext}}(k = 0) \simeq 8 \cdot 10^7$  GeV] for  $b = 0.15$  [ $b = 0.32$ ]. We observe that the obtained  $Y_{\tilde{G}}$ 's decrease with increasing  $\bar{H}_1$  (as for  $b = 0$ ) and are well below the bounds of Eqs. (A.1) and (A.2) besides for  $b = 0.32$ ,  $m_{\tilde{G}} = 0.67$  TeV and



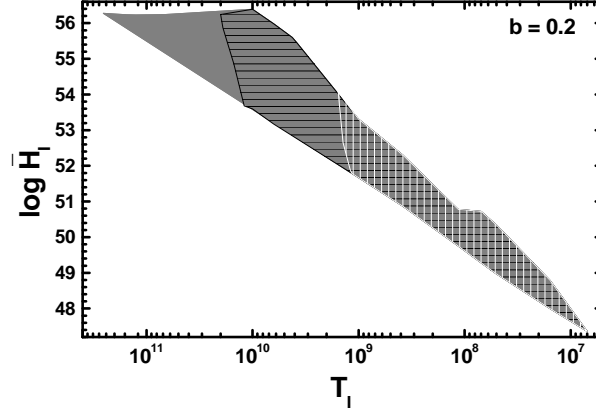


**FIGURE 9:** Regions in the  $T_1 - \log \bar{H}_1$  plane that are simultaneously allowed by the quintessential requirements (gray shaded area) – Eqs. (2.13)-(2.17) – and the  $\tilde{G}$  constraint for  $M_{1/2} = 1$  TeV,  $m_{\tilde{G}} = 0.5$  TeV and  $B_h = 0.001$  (black lined area) or  $B_h = 1$  (white lined area). We take  $a = 0.5$ ,  $b = 0.2$  and  $\bar{q}_1 = 0.01$ .

$B_h = 1$  where  $Y_{\tilde{G}}$  marginally violates the relevant bound. As a consequence, the  $\tilde{G}$  constraint can be comfortably eluded for the  $(b, \bar{H}_1)$ 's used in Fig. 4 and 5 since the employed there  $\bar{H}_1$ 's belong in the ranges of  $\bar{H}_1$  examined in Table 2-(b). Comparing the results of Table 2-(a) and (b) we remark that evading the  $\tilde{G}$  constraint requires larger  $\bar{H}_1$ 's for  $b \neq 0$  than for  $b = 0$  – see, e.g., the entries of two tables for  $m_{\tilde{G}} = 0.67$  TeV and  $B_h = 1$ .

The importance of the KD era in weakening the  $\tilde{G}$  constraint within our QS can be also induced by Fig. 9, where, in contrast to our previous approach,  $T_1$  is variable, whereas  $m_{\tilde{G}}$  is fixed to a representative value. Namely, in Fig. 9, we show the regions in the  $\log T_1 - \log \Omega_q^{\text{BBN}}$  plane that are allowed by the quintessential requirements – see Fig. 2-(b) –, for  $m_{\tilde{G}} = 0.5$  TeV,  $M_{1/2} = 1$  TeV and  $B_h = 0.001$  (black lined area) or  $B_h = 1$  (white lined area). We observe that for  $B_h = 0.001$  the allowed maximal  $T_1$  is higher than in the case of  $B_h = 1$ . This is because for  $B_h = 0.001$  we impose  $Y_{\tilde{G}}(T_{\text{BBN}}) \lesssim 1.7 \cdot 10^{-15}$ , whereas for  $B_h = 1$ , we impose  $Y_{\tilde{G}}(T_{\text{BBN}}) \lesssim 1.7 \cdot 10^{-16}$  (in accordance with Figs 1 and 2 of Ref. [63]). As a consequence, the maximal allowed  $T_{\text{ext}}(k=0) \simeq (4.8 \cdot 10^5 - 6.8 \cdot 10^6)$  GeV for  $B_h = 0.001$  is higher than the one  $(4.6 \cdot 10^4 - 5.7 \cdot 10^5)$  GeV allowed for  $B_h = 1$ . The same hierarchy holds for  $T_1$ 's too. Finally, we remark that the maximal  $\bar{H}_1$ 's depend very weakly on  $T_1$ .

Concluding, we can say that although the  $\tilde{G}$  constraint is more severe in the present QS than in the case of a pure KD era, it remains much weaker than in the case of the SC. As a consequence, relatively high values of  $T_1$  can be comfortably accommodated in both former cases.

## REFERENCES

- [1] E. KOMATSU *et al.* [WMAP COLLABORATION], *Astrophys. J. Suppl.* **180**, 330 (2009) [arXiv:0803.0547] <http://lambda.gsfc.nasa.gov/product/map/dr2/parameters.cfm>.
- [2] M. TEGMARK *et al.*, *Phys. Rev. D* **69**, 103501 (2004) [astro-ph/0310723]; A.G. RIESS *et al.*, *Astrophys. J.* **607**, 665 (2004) [astro-ph/0402512].
- [3] *For a review from the viewpoint of particle physics, see* A.B. LAHANAS *et al.*, *Int. J. Mod. Phys. D* **12**, 1529 (2003) [hep-ph/0308251].
- [4] K. MATCHEV, hep-ph/0402088; E.A. BALTZ, astro-ph/0412170; G. LAZARIDES, hep-ph/0601016; M. TAOSO, G. BERTONE AND A. MASIERO, *J. Cosmol. Astropart. Phys.* **03**, 022 (2008) [arXiv:0711.4996].

- [5] G. JUNGMAN, M. KAMIONKOWSKI AND K. GRIEST, *Phys. Rep.* **267**, 195 (1996) [hep-ph/9506380].
- [6] G. SERVANT AND T.M.P. TAIT, *Nucl. Phys.* **B650**, 391 (2003) [hep-ph/0206071];  
H.C. CHENG *et al.*, *Phys. Rev. Lett.* **89**, 211301 (2002) [hep-ph/0207125];  
K. AGASHE AND G. SERVANT, *Phys. Rev. Lett.* **93**, 231805 (2004) [hep-ph/0403143];  
J.A.R. CEMBRANOS *et al.*, *Phys. Rev. Lett.* **90**, 241301 (2003) [hep-ph/0302041].
- [7] J. McDONALD, *Phys. Rev. Lett.* **88**, 091304 (2002) [hep-ph/0106249];  
M. CIRELLI, N. FORNENGO AND A. STRUMIA, *Nucl. Phys.* **B753**, 178 (2006) [hep-ph/0512090];  
T. ASAKA, K. ISHIWATA AND T. MOROI, *Phys. Rev. D* **73**, 051301 (2006) [hep-ph/0512118];  
D.G. CERDEÑO, C. MUÑOZ AND O. SETO, *Phys. Rev. D* **79**, 023510 (2009) [arXiv:0807.3029];  
F. DEPPISCH AND A. PILAFTSIS, *J. High Energy Phys.* **10**, 080 (2008) [arXiv:0808.0490].
- [8] H. GOLDBERG, *Phys. Rev. Lett.* **50**, 1419 (1983);  
J.R. ELLIS *et al.*, *Nucl. Phys.* **B238**, 453 (1984).
- [9] K.Y. CHOI AND L. ROSZKOWSKI, *AIP Conf. Proc.* **805**, 30 (2006) [hep-ph/0511003];  
K.Y. CHOI, L. ROSZKOWSKI, R.R. DE AUSTRI, *J. High Energy Phys.* **04**, 016 (2008) [arXiv:0710.3349].
- [10] J. KIM, *Phys. Rep.* **150**, 1 (1987).
- [11] M.YU. KHLOPOV AND A.D. LINDE, *Phys. Lett. B* **138**, 265 (1984);  
J. ELLIS, J.E. KIM AND D.V. NANOPOULOS, *Phys. Lett. B* **145**, 181 (1984).
- [12] M. BOLZ, A. BRANDENBURG AND W. BUCHMÜLLER, *Nucl. Phys.* **B606**, 518 (2001);  
M. BOLZ, A. BRANDENBURG AND W. BUCHMÜLLER, *Nucl. Phys.* **B790**, 336 (2008) (E) [hep-ph/0012052];  
J. PRADLER AND F.D. STEFFEN, *Phys. Rev. D* **75**, 023509 (2007) [hep-ph/0608344].
- [13] L. COVI *et al.*, *J. High Energy Phys.* **05**, 033 (2001) [hep-ph/0101009].
- [14] A. BRANDENBURG AND F.D. STEFFEN, *J. Cosmol. Astropart. Phys.* **08**, 008 (2004) [hep-ph/0405158]  
(version of 16 March 2009).
- [15] L. COVI *et al.*, *J. High Energy Phys.* **07**, 023 (2002) [hep-ph/0206119].
- [16] V.S. RYCHKOV AND A. STRUMIA, *Phys. Rev. D* **75**, 075011 (2007) [hep-ph/0701104].
- [17] J. ELLIS, K.A. OLIVE, Y. SANTOSO AND V.C. SPANOS, *Phys. Lett. B* **588**, 7 (2004) [hep-ph/0312262];  
L. COVI *et al.*, *J. High Energy Phys.* **06**, 003 (2004) [hep-ph/0402240].
- [18] L. COVI *et al.*, *Phys. Rev. Lett.* **82**, 4180 (1999) [hep-ph/9905212].
- [19] N. YOSHIDA *et al.*, *Astrophys. J.* **591** L1 (2003) [astro-ph/0303622];  
K. JEDAMZIK *et al.*, *J. Cosmol. Astropart. Phys.* **07**, 010 (2006) [astro-ph/0508141].
- [20] M. KAMIONKOWSKI AND M.S. TURNER, *Phys. Rev. D* **42**, 3310 (1990);  
C. PALLIS, “The Identification of Dark Matter”, pp. 602-608 [hep-ph/0610433].
- [21] G.F. GIUDICE, E.W. KOLB AND A. RIOTTO, *Phys. Rev. D* **64**, 023508 (2001) [hep-ph/0005123];  
C. PALLIS, *Astropart. Phys.* **21**, 689 (2004) [hep-ph/0402033];  
C. PALLIS, *Nucl. Phys.* **B751**, 129 (2006) [hep-ph/0510234];  
G.B. GELMINI AND P. GONDOLO, *Phys. Rev. D* **74**, 023510 (2006) [hep-ph/0602230];  
G. BARENBOIM AND J.D. LYKKEN, *J. High Energy Phys.* **12**, 005 (2006) [hep-ph/0608265];  
A.B. LAHANAS, N.E. MAVROMATOS AND D.V. NANOPOULOS, *Phys. Lett. B* **649**, 83 (2007) [hep-ph/0612152];  
M. DREES, H. IMINNIYAZ AND M. KAKIZAKI, *Phys. Rev. D* **76**, 103524 (2007) [arXiv:0704.1590].
- [22] R. CATENA *et al.*, *Phys. Rev. D* **70**, 063519 (2004) [astro-ph/0403614];  
R. CATENA *et al.*, *J. High Energy Phys.* **10**, 003 (2008) [arXiv:0712.3173].
- [23] B. SPOKOINY, *Phys. Lett. B* **315**, 40 (1993) [gr-qc/9306008];  
M. JOYCE, *Phys. Rev. D* **55**, 1875 (1997) [hep-ph/9606223];  
P.G. FERREIRA AND M. JOYCE, *Phys. Rev. D* **58**, 023503 (1998) [astro-ph/9711102].
- [24] P. SALATI, *Phys. Lett. B* **571**, 121 (2003) [astro-ph/0207396].

- [25] S. PROFUMO AND P. ULLIO, *J. Cosmol. Astropart. Phys.* **11**, 006 (2003) [hep-ph/0309220];  
D.J.H. CHUNG *et al.*, *J. High Energy Phys.* **10**, 016 (2007) [arXiv:0706.2375].
- [26] C. PALLIS, *J. Cosmol. Astropart. Phys.* **10**, 015 (2005) [hep-ph/0503080].
- [27] R.R. CALDWELL *et al.*, *Phys. Rev. Lett.* **80**, 1582 (1998) [astro-ph/9708069].
- [28] P. BINETRUI, *Int. J. Theor. Phys.* **39**, 1859 (2000) [hep-ph/0005037];  
E.J. COPELAND *et al.*, *Int. J. Mod. Phys. D* **15**, 1936 (2006) [hep-th/0603057].
- [29] P.J. PEEBLES AND A. VILENKIN, *Phys. Rev. D* **59**, 063505 (1999) [astro-ph/9810509];  
M. PELOSO AND F. ROSATI, *J. High Energy Phys.* **12**, 026 (1999) [hep-ph/9908271].
- [30] K. DIMOPOULOS AND J.W. VALLE, *Astropart. Phys.* **18**, 287 (2002) [astro-ph/0111417];  
K. DIMOPOULOS, *Phys. Rev. D* **68**, 123506 (2003) [astro-ph/0212264];  
I.P. NEUPANE, *Class. Quant. Grav.* **25**, 125013 (2008) [arXiv:0706.2654];  
M. BASTERO-GIL, A. BERERA, B.M. JACKSON AND A. TAYLOR, *Phys. Lett. B* **678**, 157 (2009) [arXiv:0905.2937].
- [31] D.J.H. CHUNG, L.L. EVERETT AND K.T. MATCHEV, *Phys. Rev. D* **76**, 103530 (2007) [arXiv:0704.3285];  
G. BARENBOIM AND J.D. LYKKEN, *J. High Energy Phys.* **10**, 032 (2007) [arXiv:0707.3999].
- [32] M.E. GÓMEZ *et al.*, *J. Cosmol. Astropart. Phys.* **01**, 027 (2009) [arXiv:0809.1859];  
M.E. GÓMEZ *et al.*, *AIP Conf. Proc.* **1115**, 157 (2009) [arXiv:0809.1982].
- [33] C. WETTERICH, *Nucl. Phys.* **B302**, 668 (1988).
- [34] E.J. COPELAND, A.R. LIDDLE AND D. WANDS, *Phys. Rev. D* **57**, 4686 (1998) [gr-qc/9711068];  
E.J. COPELAND, N.J. NUNES AND F. ROSATI, *Phys. Rev. D* **62**, 123503 (2000) [hep-ph/0005222].
- [35] U. FRANÇA AND R. ROSENFELD, *J. High Energy Phys.* **10**, 015 (2002) [astro-ph/0206194];  
C.L. GARDNER, *Nucl. Phys.* **B707**, 278 (2005) [astro-ph/0407604]; hep-ph/0701036.
- [36] P.J. STEINHARDT, L. WANG AND I. ZLATEV, *Phys. Rev. Lett.* **82**, 896 (1999) [astro-ph/9807002];  
*ibid.*, *Phys. Rev. D* **59**, 123504 (1999) [astro-ph/9812313].
- [37] B. RATRA AND P.J.E. PEEBLES, *Phys. Rev. D* **37**, 3406 (1988);  
A.R. LIDDLE AND R.J. SCHERRER, *Phys. Rev. D* **59**, 023509 (1999) [astro-ph/9809272];  
J.P. UZAN, *Phys. Rev. D* **59**, 123510 (1999) [gr-qc/9903004].
- [38] P. BINETRUY, *Phys. Rev. D* **60**, 063502 (1999) [hep-ph/9810553];  
P. BINETRUY, *Supersymmetry*, Oxford University Press (2006).
- [39] A. MASIERO, M. PIETRONI AND F. ROSATI, *Phys. Rev. D* **61**, 023504 (2000) [hep-ph/9905346];  
F. ROSATI, *Phys. Lett. B* **570**, 5 (2003) [hep-ph/0302159].
- [40] M. DINE, L. RANDALL AND S.D. THOMAS, *Phys. Rev. Lett.* **75**, 398 (1995) [hep-ph/9503303];  
D.J.H. CHUNG, L.L. EVERETT AND A. RIOTTO, *Phys. Lett. B* **556**, 61 (2003) [hep-ph/0210427].
- [41] P. BRAX *et al.*, *J. Cosmol. Astropart. Phys.* **09**, 032 (2009) [arXiv:0904.3471].
- [42] S.D. H. HSU AND B. MURRAY, *Phys. Lett. B* **595**, 16 (2004) [astro-ph/0402541];  
D.J. LIU AND X.Z. LI, *Phys. Lett. B* **611**, 8 (2005) [astro-ph/0501596];  
W.Z. LIU AND D.J. LIU, *Int. J. Mod. Phys. D* **18**, 43 (2009) arXiv:0803.4039.
- [43] C. BACCIGALUPI *et al.*, *Phys. Rev. D* **65**, 063520 (2002) [astro-ph/0109097].
- [44] R.H. CYBURT *et al.*, *Astropart. Phys.* **23**, 313 (2005) [astro-ph/0408033].
- [45] R. BEAN, S.H. HANSEN AND A. MELCHIORRI, *Phys. Rev. D* **64**, 103508 (2001) [astro-ph/0104162].
- [46] G. BÉLANGER *et al.*, *Comput. Phys. Commun.* **149**, 103 (2002) [hep-ph/0112278];  
P. GONDOLO *et al.*, *J. Cosmol. Astropart. Phys.* **07**, 008 (2004) [astro-ph/0406204].
- [47] M.R. DE GARCIA MAIA, *Phys. Rev. D* **48**, 647 (1993);  
M.R. DE GARCIA MAIA AND J.D. BARROW, *Phys. Rev. D* **50**, 6262 (1994).

- [48] M. GIOVANNINI, *Phys. Rev. D* **60**, 123511 (1999) [astro-ph/9903004];  
V. SAHNI, M. SAMI AND T. SOURADEEP, *Phys. Rev. D* **65**, 023518 (2002) [gr-qc/0105121].
- [49] T.L. SMITH, M. KAMIONKOWSKI AND A. COORAY, *Phys. Rev. D* **73**, 023504 (2006) [astro-ph/0506422].
- [50] G. LAZARIDES, R.K. SCHAEFER, AND Q. SHAFI, *Phys. Rev. D* **56**, 1324 (1997) [hep-ph/9608256].
- [51] J. HISANO *et al.*, *Phys. Rev. D* **79**, 083522 (2009) [arXiv:0901.3582].
- [52] S. GALLI, F. IOCCO, G. BERTONE AND A. MELCHIORRI, *Phys. Rev. D* **80**, 023505 (2009) [arXiv:0905.0003];  
T.R. SLATYER, N. PADMANABHAN AND D.P. FINKBEINER, *Phys. Rev. D* **80**, 043526 (2009) [arXiv:0906.1197].
- [53] S. CHANG AND H.B. KIM, *Phys. Rev. Lett.* **77**, 591 (1996) [hep-ph/9604222];  
M. KAWASAKI *et al.*, *J. Cosmol. Astropart. Phys.* **03**, 009 (2008) [arXiv:0711.3083].
- [54] K. RAJAGOPAL, M.S. TURNER AND F. WILCZEK, *Nucl. Phys.* **B358**, 447 (1991).
- [55] A.A.E. ZANT, S. KHALIL AND H. OKADA, arXiv:0903.5083;  
W.L. GUO AND X. ZHANG, *Phys. Rev. D* **79**, 115023 (2009) [arXiv:0904.2451];  
J. McDONALD, arXiv:0904.0969.
- [56] O. ADRIANI *et al.* [PAMELA COLLABORATION], *Nature* **458**, 607 (2009) [arXiv:0810.4995];  
J. CHANG *et al.* [ATIC COLLABORATION], *Nature* **456**, 362 (2008);  
A.A. ABDO *et al.* [THE FERMI-LAT COLLABORATION], *Phys. Rev. Lett.* **102**, 181101 (2009) [arXiv:0905.0025].
- [57] M. IBE, H. MURAYAMA AND T.T. YANAGIDA, *Phys. Rev. D* **79**, 095009 (2009) [arXiv:0812.0072];  
W.L. GUO AND Y.L. WU, *Phys. Rev. D* **79**, 055012 (2009) [arXiv:0901.1450].
- [58] J. HISANO, S. MATSUMOTO, M.M. NOJIRI AND O. SAITO, *Phys. Rev. D* **71**, 063528 (2005) [hep-ph/0412403];  
N. ARKANI-HAMED *et al.*, *Phys. Rev. D* **79**, 015014 (2009) [arXiv:0810.0713];  
M. LATTANZI AND J.I. SILK, *Phys. Rev. D* **79**, 083523 (2009) [arXiv:0812.0360];  
J.D. MARCH-RUSSELL AND S.M. WEST, *Phys. Lett. B* **676**, 133 (2009) [arXiv:0812.0559];  
X.G. HE, arXiv:0908.2908.
- [59] D. HOOPER, *et al.*, *J. Cosmol. Astropart. Phys.* **01**, 025 (2009) [arXiv:0810.1527];  
H. YUKSEL, M. D. KISTLER AND T. STANEV, arXiv:0810.2784.
- [60] C. PALLIS, *Nucl. Phys.* **B831**, 217 (2010) [arXiv:0909.3026].
- [61] D.H. LYTH AND T. MOROI, *J. High Energy Phys.* **05**, 004 (2004) [hep-ph/0402174].
- [62] E.J. CHUN AND S. SCOPEL, *J. Cosmol. Astropart. Phys.* **10**, 011 (2007) [arXiv:0707.1544];  
M.C. BENTO *et al.*, *Phys. Rev. D* **73**, 023506 (2006) [hep-ph/0508213];  
N. OKADA AND O. SETO, *Phys. Rev. D* **73**, 063505 (2006) [hep-ph/0507279].
- [63] M. KAWASAKI, K. KOHRI AND T. MOROI, *Phys. Lett. B* **625**, 7 (2005) [astro-ph/0402490].
- [64] M. KAWASAKI, K. KOHRI AND T. MOROI, *Phys. Rev. D* **71**, 083502 (2005) [astro-ph/0408426];  
M. KAWASAKI, K. KOHRI, T. MOROI AND A. YOTSUYANAGI, *Phys. Rev. D* **78**, 065011 (2008) [arXiv:0804.3745].
- [65] R.H. CYBURT *et al.*, *Phys. Rev. D* **67**, 103521 (2003) [astro-ph/0211258];  
J.R. ELLIS, K.A. OLIVE AND E. VANGIONI, *Phys. Lett. B* **619**, 30 (2005) [astro-ph/0503023].